Title
A STUDY OF THE PICK-UP PROCESS IN PROTON-DEUTERON SCATTERING

Author
Bratenahl, Alexander.

Publication Date
1952-06-02

UCRL -1842
Cy. 2

UNIVERSITY OF CALIFORNIA

Ernest O. Lawrence Radiation Laboratory

BERKELEY, CALIFORNIA

DISCLAIMER

UCRL-1842
Unclassified-Physics Distribution

UNCLASSIFIED

UNIVERSITY OF CALIFORNIA

Radiation Laboratory

Contract No. W-7405-eng-48

A STUDY OF THE PICK-UP PROCESS IN PROTON-DEUTERON SCATTERING

Alexander Bratenahl

(Thesis)

June 2, 1952

Berkeley, California

TABLE OF CONTENTS

I. INTRODUCTION AND STATEMENT OF PROBLEM

It has been observed by Hadley and York[1], and by others[2][3] that nuclear bombardments by 90 Mev neutrons result in an unexpectedly large yield of deuterons of an energy of the same order as the incident neutrons. These deuterons, moreover, are found sharply peaked forward in angular distribution. The large yield, the energy, and the angular distribution strongly suggest a production mechanism more direct than the usual decay of an intermediate compound nucleus[4]. Chew and Goldberger[5] have proposed a process involving a sudden rearrangement collision in which a proton is transferred from the target nucleus to the passing neutron. They have given the name "pick-up" to this type of transfer process, which, of course, is equally applicable in case the role of proton and neutron is reversed. Heidmann[6] has extended the calculations of Chew and Goldberger[5], and both calculations show reasonably good agreement with York's data.

Superficially, deuteron pick-up is the inverse of the type of deuteron stripping described by Serber[7], but contains in its calculation one important element that is not present in the case of stripping. The pick-up process, unlike stripping, imposes a condition on the momentum the struck particle possessed at the instant of collision. Indeed, the probability of producing a deuteron of a particular momentum $\vec{K}$ by an incident nucleon of momentum $\vec{k}$ depends on the probability of finding a collision partner of momentum $(\vec{K}-\vec{k})$ in the nucleus. This simple relation is neither sufficient nor necessary; unfortunately, it may happen that in the collision some momentum is transferred to a third nucleon. Moreover, the momentum $\vec{k}$ of the incident particle is the momentum

possessed just prior to the pick-up collision and may have been changed from the observable incident momentum by previous interactions in the nucleus. But if the assumption is made that the entire collision between incident particle and target is confined to the single interaction of the two particles observed as an emerging deuteron, then the pick-up process becomes a useful method of determining the momentum distribution, $N(\vec{K}-\vec{k})$, of nucleons in a nucleus.

Of course, what is termed momentum distribution $N(\vec{K}-\vec{k})$ is meant here the square of the magnitude of the Fourier transform of the nuclear wave function, and the pick-up calculations of Chew[5] involve a Born approximation of the scattering amplitudes corresponding to the momentum transfer indicated above. Besides the distribution $N(\vec{K}-\vec{k})$ there occurs also in this calculation an integration over all the amplitudes of relative momenta in the emerging deuteron. Thus, the deuteron wave function is supposed already known from theory in order to apply the pick-up calculation to the general case.

A systematic study of the momentum distribution in nuclei by the use of the pick-up process therefore depends on the extent or range of validity of the single interaction assumption. There is growing evidence that in high energy nuclear bombardments a substantial fraction of collisions involve single interactions of nucleons. Thus the work of Cladis[8] on the observation of inelastically scattered protons by nuclei show broad peaks in energy which follow the $\cos^2\Phi$ law with angle signifying single nucleon encounters and is considered evidence for quasi-elastic scattering. Moreover, the shape of the peaks yield, according to Wolf's analysis[9], momentum distributions of nucleons which seem to

provide sensible interpretation of meson production spectra[10].

A striking demonstration of the single nucleon-nucleon character of high energy collisions is seen in the observation of Chamberlain[11] on the angular correlation of proton pairs emerging from Li^7 under 340 Mev proton bombardment. Here, however, the momentum requirements in the collision are different than in the pick-up process leading to deuteron formation in that the final relative momentum is an observable while in the case of the bound deuteron it is not. Nevertheless, in this case as in the pick-up process the incident proton momentum $\vec{k}$ and the center of mass momentum $\vec{K}$ of the emerging pair determine the momentum the struck nucleon possessed in the nucleus.

It is not entirely surprising that nucleon-nucleon collision phenomena should characterize, to a considerable extent, high energy collisions with nuclei, for the de Broglie wave length of even a 90 Mev neutron is much smaller than a nucleus (1/19 for Pb) as is demonstrated, for example, in the diffraction scattering of 90 Mev neutrons[12]. Indeed, the wave length of such particles is of the order of the proper volume of single nucleons in the nucleus. Single nucleon encounters are likely since the mean free path in the nucleus, deduced by Fernbach[13] from neutron absorption cross sections is of the order of the radius of light nuclei. There is then some hope that the single interaction assumption might be acceptable to a sufficient degree to permit determination of momentum distributions from a study of pick-up produced deuterons.

Both the angular distribution and the energy dependence of the pick-up cross section depend on $N(\vec{K} - \vec{k})$. Although this distribution function is in general not known <u>à priori</u>, the measurement of both the

angular distribution and energy dependence provide a critical test of the pick-up hypothesis[5].

Perhaps the simplest nucleus to investigate is the case in which the target nucleus is itself a deuteron for in this case $N(\vec{R}-\vec{k})$ is moderately well determined by theory[14]. The momentum relations in this case lead to an interesting conclusion. The magnitude of the momentum of the proton left behind.

$$|\vec{R}-\vec{k}| = \sqrt{K^2 + k^2 - 2Kk\cos\Phi} \tag{1}$$

and under the single interaction assumption alluded to above is equal to the magnitude of the momentum of the struck target neutron. The magnitude of the momentum relative to the center of mass of the collision partners is

$$|\vec{k} - \vec{K}/2| = \sqrt{k^2 + \frac{K^2}{4} - kK\cos\Phi} \tag{2}$$

On the other hand, momentum conservation yields

$$K = \frac{4}{3}k\cos\Phi \tag{3}$$

and using (3) to eliminate Φ from (1) and (2) one sees that

$$|\vec{R}-\vec{k}| = |\vec{k}-\vec{K}/2| \tag{4}$$

Referring now to Reference (5), and entering this result in the magnitude of the squared matrix element for the transition given in Equation (8) of that paper:

$$|H|^2 = N(K-k)\left|\varphi_d(\vec{k}-\vec{K}/2)\right|^2\left[B_d - \frac{\hbar^2}{M}(\vec{k}-\vec{K}/2)^2\right]^2 \tag{5}$$

It is apparent that the transition probability is proportional to the fourth power of the magnitude of the Fourier component φ_d of the deuteron wave function corresponding to the momentum magnitude $|\vec{R}-\vec{k}|$, the laboratory momentum of the scattered proton.

The pick-up deuterons will appear as recoils resulting from the elastic scattering of protons into very large angles. Although there is some ambiguity as to what is pick-up and what is characterized by other processes, it is felt that pick-up dominates at large proton angles where the contribution of other processes is small[15][16]. Coon, Tascheck and Forbes[17] have studied neutron deuteron elastic scattering at 14 Mev and observe a distinct peak of recoil deuterons in the forward direction where the half-width agrees well with that predicted by Chew and Goldberger[5], even though the neutron energy is too low for these calculations to be reliable. Hadley[18] has observed these deuterons in neutron-deuteron scattering at 270 Mev. Stern[19] has observed this same peak in the scattering of 180 Mev deuterons by protons. In this case, however, the resulting cross section is smaller by a factor of five from that predicted[5]. Powell[20], making observations in the cloud chamber, finds results equivalent to Stern.

Jastrow and Karp[31] have considered this discrepancy as evidence of a failure of the single interaction assumption under these conditions. The relatively high momentum components, $\vec{R}-\vec{k}$, involved are considered to be associated with small neutron-proton separation distances in the deuteron, well inside the range of nuclear forces. If this is true, then of course, momentum is transferred to both target nucleons and the pick-up amplitude is complicated by three-body considerations.

It is the purpose of this paper to report on some studies of proton-deuteron scattering at several energies in the angular region presumably dominated by pick-up with the intention of providing evidence for determining to what degree the pick-up hypothesis is valid. This study also serves to extend the experimental evidence on proton-deuteron scattering which is of fundamental importance to the understanding of nuclear forces. (See, for example, Reference 15).

II. GENERAL EXPERIMENTAL METHOD

The angular half width of the forward peak of recoil deuterons is of the order of 10° to the incident beam, and it is desirable to make observation at smaller angles particularly in the direction of the beam itself. The experiment is, therefore, conducted in the magnetic field of the 184 inch Berkeley synchrocyclotron where use is made of the field to deflect the deuterons through large angles into a detector. The momentum of recoil deuterons making an angle Φ with the direction of incident protons of momentum $\vec{k}$ is $\frac{4}{3}k\cos\Phi$. In terms of radius of curvature ρ of the incident protons, the radius of curvature of the recoil deuterons is $\frac{4}{3}\rho\cos\Phi$.

Provided the magnetic deflection angle is close to 180°, there is a limited range about $\Phi=0^{\circ}$ in which a detector may receive these deuterons at a cyclotron radius well outside the envelope of all orbits of protons scattered by the target (Fig. 1). The complication of permitting deuteron orbits to pass into the fringing field of the magnet where the perturbation of regular orbits becomes a serious computational problem is avoided at the expense of restricting the maximum radius of curvature of observed deuterons. This limit, in terms of incident proton energy, is 150 Mev for observation of recoil deuterons at $\Phi = 0^{\circ}$. Practical limitations imposed by such other matters as the length and location of available probes in the cyclotron, the difficulty of placing detectors above or below the circulating proton beam, and so on, place other restrictions on the range of possible observations in energy and angle (Fig. 2).

The targets used in this experiment are deuterated paraffin, $(CD_2)x$, and polyethylene, $(CH_2)x$. The difference in deuteron yield of

these two targets is then taken as the yield from deuterium. The C^{11} activity induced in the target by the proton bombardment is utilized to monitor the incident proton beam.

The particles received from the target are detected by observing their tracks in nuclear photographic emulsions. To establish the identify of a particle it is sufficient to measure both its momentum and energy, or any pair of quantities that are related to momentum and energy in different ways. In this experiment, identification is accomplished by the combination $H\rho$ and range. According to York[1] a good approximation of the relation of the range R of a particle of mass m, charge q to its kinetic energy E may be expressed in the energy range of interest by

$$R = \frac{K'}{q^2 m^{0.8}} E^{1.8}$$

where K' characterizes the stopping material. On the other hand, momentum, energy and $H\rho$ are connected by:

$$E = \frac{P^2}{2m} = \frac{(H\rho)^2}{2c^2}\frac{q^2}{m}$$

For fixed $H\rho$ the ratio of ranges of particles of masses m_1, m_2 and charges of q_1, q_2 is easily seen from the above relations to be:

$$\left(\frac{R_1}{R_2}\right)_{H\rho \text{ fixed}} = \left(\frac{m_2}{m_1}\right)^{2.6}\left(\frac{q_1}{q_2}\right)^{1.6}$$

Likewise, the ratio of $H\rho$'s for fixed range is given by:

$$\left(\frac{H\rho_1}{H\rho_2}\right)_{\text{range fixed}} = \left(\frac{m_1}{m_2}\right)^{.72}\left(\frac{q_2}{q_1}\right)^{.44}$$

Taking the deuteron as particle 2 these ratios are given for other possible particles in Table I.

TABLE I

	P	D	T	He^3	α
$\left(\frac{R_1}{R_2}\right)$ $H\rho$ fixed	6.1	1	.35	1.06	.50
$\left(\frac{H\rho_1}{H\rho_2}\right)$ R fixed	.61	1	1.34	.99	1.21

From the ratio of ranges, it is seen that range and $H\rho$ afford good discrimination against other particles leaving the target with the exception of He^3. Since the observations on deuterons are made at energies of the order 8/9 the incident proton energy, protons, He^3's, and α's would require production energies of the order of 1.8, 2.3, and 1.8 times the incident energy to be detected. These particles are, therefore, not to be expected for energetic reasons. Only tritons, therefore, can be present along with the protons and deuterons. Spurious sources of particles in the cyclotron are less well discriminated against because in general their $H\rho$ will not be known. However, from the ratio of $H\rho$'s at fixed range, well-localized sources can be identified.

III. DETAILS OF EXPERIMENTAL METHOD

A. Proton Beam

As is well known, the circulating beam in a synchrocyclotron, as received on an internal target, is generally neither homogenous in energy nor in direction [21, 22, 23]. Fortunately, the directional inhomogeneity is small. The spread in energy, however, is a serious difficulty in conducting an experiment of this kind and must be taken into account. It will be seen in what follows (Section V, B; also Fig. 3) that the actual energy spectrum of the internal proton beam is furnished as a by-product of the experimental measurements, and the half width of the spectrum turns out to be of the order of 10% of the mean incident energy. The energy spread is produced by three principal factors: (1) free radial oscillations in the proton orbits; (2) multiple passage of the beam through the target; (3) energy loss in the target itself. The last two factors are interrelated, controllable, and are minimized to such an extent that the 10% width referred to above is believed to be almost solely due to radial oscillations.

The method of control employed involves a balance between energy loss in the target, which is kept small, and small angle multiple scattering which is made as large as possible relative to an aperture which severely clips the beam in vertical section. Since a choice of energy loss fixes the small angle scattering (see, for example, Rossi, and Greison[24]) the control is actually effected as a balance between energy loss and clipper aperture. The theory of this procedure is amply discussed and demonstrated in a paper by Knox[25]. This procedure makes it

possible to use targets less than 1% thick in energy and at the same time, restrict multiple passage to the extent that less than 2% of the beam passes through the target a second time.

All attempts at controlling the residual spread in proton energy, presumably due to free radial oscillations, have so far failed and the experiment is conducted and interpreted keeping this energy spread in mind.

Free radial oscillations is the term applied to the horizontal perturbation of ion orbits. The frequency of this motion, ω_r, depends on the radial decrease in magnetic field. This radial decrease is conveniently expressed in terms of n, defined as:

$$n = -\frac{r}{H}\frac{\partial H}{\partial r}$$

Bohm and Foldy[26] in developing the theory of the synchrocyclotron, show that the perturbed motion for small n and small perturbations Δr and ΔZ on the normal equation of motion of ions may be expressed in cylindrical coordinates as

$$\left.\begin{aligned} \Delta\ddot{r} + (1-n)\omega_0^2 \Delta r &= 0 \\ \Delta\ddot{z} + n\omega_0^2 \Delta z &= 0 \end{aligned}\right\} \quad 0 < n < 1$$

with

$$\omega_0 = \frac{eH}{mc}$$

The effect of this perturbation on the energy an ion possesses at the time it strikes an internal cyclotron target may be seen on consideration of three principal frequencies involved in the ion motion parallel to the magnetic median plane: the fundamental synchrocyclotron

frequency, $\omega_o(t)$, the radial oscillation frequency, $\omega_r = \sqrt{1-n}\,\omega_o$; and the difference or precessional frequency $\omega_{prc} = (1 - \sqrt{1-n})\omega_o$. These three frequencies result in a trochoidal motion for the ion. The center of curvature of the ion precesses in the direction of the ion motion in a circle of radius Δr_o about the magnetic field center at the frequency $(1 - \sqrt{1-n})\omega_o$, causing the apse or point of maximum radial excursion to precess also about this center at the same frequency. Thus, viewed at a fixed azimuth, successive transits of the ion appear at a sinusoidally varying radius. At the same time, the radius of curvature ρ of the ion and hence also the mean radius of the ion $\bar{r}$ is increased in small increments ΔE_v by the aquisition of energy from the radiofrequency field in the dee gap. It is clear, then, that an ion possessing an amplitude Δr_o of radial oscillation will tend to strike the target at a time when the orbit apse is approaching and makes a small angle δ with the azimuthal coordinate of the target. If r_T is the target radius, one has the approximate relation

$$\rho = r_T - \Delta r_o \cos\delta$$

Since the ion-energy is determined by ρ, the ion always "cheats" and arrives at the target with less energy than the proper synchronous orbit energy E_T at the radius r_T. In fact,

$$E \approx E_T \left(1 - \frac{2\Delta r_o \cos\delta}{r_T}\right)$$

(The situation is depicted in Fig. 4.) The maximum angle δ is approximately given by:

$$\delta^2 = \frac{\omega_o}{\omega_{prc}} \frac{\Delta r_T}{\Delta r_o} \frac{\Delta E_v}{E_T}$$

In these experiments, $r_T \sim 45''$ $\Delta E_V \sim 10^4$, $n = 0.031$. The mean Δr_o is found to be $\sim 3''$ so that $\delta \leq 18^\circ$. The maximum angle ϵ_{max} at which an ion strikes a target is given by:

$$\epsilon_{max} = \frac{\Delta r_o}{r} \delta \leq 1.2^\circ$$

The angle ϵ must fall in the range $0 \leq \epsilon \leq \epsilon_{max}$ and is considered negligible in these experiments.

It should be remarked that out of the fundamental phase stability condition of synchrocyclotron theory, the consequent phase oscillations may produce large oscillation in radius and energy but that these oscillations are not of a nature to effect the energy spread of ions on a probe directly. Instead, their effect determines the incremental energy gain ΔE_V in transit of the dee gap

$$\Delta E_V = eV \sin\varphi$$
$$\ddot{\varphi} \approx \omega_\varphi^2 \varphi \qquad \text{(very approximately)}$$

Where φ is the phase angle, V is the radiofrequency dee voltage, and ω_φ is the phase oscillation frequency which is much smaller than the frequency associated with free radial oscillations. It is clear, then, that the effect of variation in ΔE_V is second order in its effect upon target energy essentially entering only in the value of δ. Phase stability and phase oscillations also determine to some extent the limits of a rather broad central region in the dee gap out of which it is possible for ions to be captured from the source into phase stable orbits. If

the free radial oscillations have their origin in off-center initial conditions, then cyclotron operating conditions favoring large phase oscillations might tend to permit large free radial oscillations and vice versa. No direct evidence for this effect was observed, however, in this experiment.

In addition to producing a spread in energy, radial oscillations also cause the ions to strike the target over a small region of radial extent ΔW given by

$$\Delta W = - \Delta r_o \delta \Delta \delta$$

with

$$\Delta \delta = -2\pi \frac{\omega_{pr+}}{\omega_o}$$

This "radial width" of the circulating beam has little effect on the resolution problem in this experiment but was found to be useful in several ways, such as, a rough check on the radial oscillations for comparison with that inferred from the energy spectrum; a means of identifying primary as compared to secondary and multiple passage of the target; and as a means of obtaining a greater total current through the paraffin target without attendant melting from high current density.

The quantity ΔW has been frequently measured during the course of these experiments in making alignment of the clipper. Providing the beam current is kept sufficiently low so as not to produce excessive heating, it is found that thin pieces of glass are blackened by the beam in such a way that the intensity I of light transmitted by the glass is related to the proton beam current P

$$I = I_o e^{-\mu P}$$

ΔW turns out to be $\sim$ 0.12 inch, but varies slightly from day to day under various cyclotron operating conditions. A maximum radial oscillation amplitude of 6 inches makes ΔW= 0.136 inch. Such amplitudes are inferred from the deuteron momentum spectrum, for example, as shown in Fig. 3.

B. Target and Monitor System

The targets used in this experiment are, as noted above, deuterated paraffin, $(CD_2)x$, serving effectively as a deuterium target containing C for monitor purposes, and polyethylene $(CH_2)x$ in order to determine the contribution of deuteron production in the carbon of the first target. The choice of polyethylene is dictated by the need for matching both energy loss and small angle scattering in the two targets. The targets are mounted together on a device which permits their interchange into the beam position without the necessity of withdrawing the assembly from the cyclotron vacuum system. This convenience is actually felt to be a necessity in this case as the target mount also serves as the adjustable clipper aperture, and for reliable subtraction purposes it is desirable not to disturb this aperture between pairs of runs requiring subtraction. The adjustment of the clipper aperture is critical, and slight changes in its alignment might involve sampling different radial oscillation amplitude distributions out of the total beam.

Although it might seem on first sight that the clipper should be located as far away as possible from the target, the chosen location turns out to be the more desirable. The beam entering the clipper is

already pre-clipped by a copper fin device located at a small radius where the proton energy is low (Fig. 1). The scattered protons and charged degradation products involved in this pre-clipping are confined by their small radius of curvature to the central region of the cyclotron. The fin is adjusted so that the beam entering the clipper aperture is only slightly broader in vertical extent than the aperture itself. The clipper then serves, through many thousands of transits, to produce a beam well collimated in vertical section. Its principal use, however, is to prevent ions from passing through the target a second time if they have suffered a change of direction in the vertical plane greater than $d/2\pi r$, d being the clipper aperture.

The r.m.s. projected scatter angle θ_o for protons in the target is 0.05 radians, on the other hand, the clipper aperture is usually $\frac{1}{4}$ inch which at 45 inch radius subtends an angle $\theta = 0.0009$ radians, therefore, the probability of passing a proton a second time is

$$P = \frac{1}{\theta_o \sqrt{2\pi}} 2\theta \approx 0.013$$

or 1.3%.

Because of its location in the general layout (Fig. 1), the clipper cannot scatter protons directly into the detector system, a fact that would not be the case for any other possible location. The principal disadvantage of placing the targets adjacent to the exit side of the clipper is the possible activation of carbon in the target and of copper in the target holder by unwanted spray. This effect, along with neutron activation of the idle target of the pair amounts to 2% of the total activation. The effect was determined by passing a beam through one

target and subsequently measuring the activity in both, as well as the target holders with the targets removed.

The monitor system involves the relative measurement of C^{11} activity induced in C^{12} by proton bombardment through the well known C^{12} (p,pn) C^{11} reaction. It has been observed by many workers that C^{11} production serves well as a monitor as there are no other decay products produced along with C^{11} in sufficient amount to interfere with an unambiguous interpretation in terms of the single decay period. Moreover, C^{11} decays by positron emission, maximum energy 0.97 Mev 20.5 minute half-life[27] and with the high level activity dealt with in this experiment, the measurement of the annihilation γ-radiation of the positrons instead of the positrons themselves, possesses the advantage of suppressing the effect of variation in self-absorption and geometry that is likely to be present in different targets. The activity is determined by measuring the ionization of Compton secondaries produced by the annihilation radiation in the walls of a tantalum-lined ionization chamber.

The ionization chamber and associated electrometer is calibrated for this purpose in an auxiliary experiment utilizing the well collimated high current beam of the Berkeley 32 Mev proton linear accelerator. The calibration consists in measuring the activity in a thin polyethylene foil and at the same time, determining the absolute proton current producing this activity by the use of a Faraday cup. The absolute yield, Y, of C^{11} produced in a target containing N atoms of carbon per square centimeter by Q/e protons of energy E in a bombardment at constant proton current of duration t is:

$$Y = \left(N \frac{Q}{e}\right) \sigma_{ppn}(E) \left[\frac{1-e^{-\lambda t}}{\lambda t}\right] \qquad (6)$$

where $\sigma_{p,pn}(E)$ is the p,pn cross section at the energy E, and λ is the decay constant of C^{11}. What is desired of the monitor system is the determination of the quantity $\left(\frac{NQ}{e}\right)$ from the measured activity A(t) referred to the time of termination of the bombardment. The calibration then essentially determines the proportionality constant, K_o (the specific property of the activity measuring device) between absolute yield and activity. In the calibration, the charge Q carried by the proton current is collected by the Faraday cup and is transferred to a condenser of accurately known capacitance C where the resulting potential is measured by a sensitive recording electrometer. Since the beam current of the linear accelerator tends to fluctuate, a resistor is adjusted across the condenser such that the RC product matches the C^{11} decay constant λ. If quantities referring to this calibration experiment are denoted by the subscript c one has the relations

$$Y = K_o A_c(t_c) = \frac{N_c Q'_c(t_c)}{e} \sigma_{ppn}(E_c) \qquad (7)$$

defining and determining the calibration constant K_o. Here, $Q'(t_c)$ is the charge measured on the condenser at the same time t_c to which the activity $A_c(t_c)$ is referred, and the assumption of constant beam level is no longer required. The desired monitor quantity, $\left(\frac{NQ}{e}\right)$, is:

$$\frac{NQ}{e} = \frac{K_o A t_o}{\sigma_{ppn}(E)} \left[\frac{\lambda t}{1-e^{-\lambda t}}\right] \qquad (8)$$

On eliminating the calibration constant,

$$\frac{NQ}{e} = \frac{N_c Q_c'}{e}\left(\frac{A}{A_c}\right)\frac{\sigma_{pn}(E_d)}{\sigma_{pn}(E)}\left[\frac{\lambda t}{1-e^{-\lambda t}}\right] \qquad (9)$$

is seen to depend only on the ratio of the C^{11} cross section at the two energies and not on its absolute value. This excitation function has been carefully measured at numerous points by Aamodt, Peterson, and Phillips[28] in the energy range extending from the threshold at 18 Mev up to 340 Mev. The energy range of threshold to 100 Mev has also been covered by Dr. N. M. Hintz of Harvard and agreement between these two experiments appears to be very good. The results of Dr. Hintz work has not yet been published, but is quoted in the Aamodt paper.

C. Detector System

The large magnetic deflection angle employed to separate deuterons from protons effects a rather high degree of momentum analysis. Although the deuteron recoils sought are the result of elastic collisions and, therefore, should possess a well defined momentum at a given angle, the spread in energy of the incident protons (Sec. II and Fig. 3) results in a corresponding spread in deuteron momenta. The monitor system samples all energy components of the incident spectrum, hence to define a cross section, it is necessary to account for all elastic recoil deuterons leaving the target in a definite solid angle regardless of their momentum. This fact complicates the design of the detector system in that, although a reasonable angular resolution is desirable, yet because of this momentum analysis, the deuterons sought are distributed over an extended region along the detector probe axis.

These requirements are met by distributing an array of detector units along the detector probe axis. The array of units, thirty-six in all, each possessing defined angular resolution limits as well as provision for determining the range in copper of the detected particle, constitutes that which is called the detector system.

The $H\rho$ of a detected particle is determined, on the assumption it originated in the target, by the position and orientation of the detector unit. Since the range in copper is measured, the particle's identity is known, subject only to the assumption as to its point of origin. But the array or detector system as a whole defines a relationship between range and $H\rho$ that is unique for any given point of origin, therefore the point of origin of the detected particles may be ascertained and the identity of the particles involved in this relationship proved (Section II, Fig. 5).

(1) Detector Unit

What is meant here by a "detector unit" is merely a channel milled out of a block of brass, in back of which is placed an absorber in the form of a copper wedge. The sensitive element is a nuclear photographic emulsion plate placed on the sloping side of the wedge (Fig. 6). The use of channels and wedges or tapered absorbers in nuclear emulsion technique is common, but it is tempting to name the combination used here a "detector" on the basis of its properties and from the method of scanning the plates.

The channel serves to select, out of all particles crossing the detector probe axis at a particular point r, those crossing at angles within a range $\Delta\alpha$ of some selected angle α as determined by the

orientation of the channel. As mentioned above, particles of each kind entering the channel have well definied $H\rho$ and range. Therefore, a track count in a swath of the emulsion extending in the direction of increasing thickness of copper absorber is equivalent to an integral bias curve, familiar in particle counter technique, and exhibits discontinuities at points where the range of various kinds of particles is exceeded (Fig. 7).

Actually, because of small angle multiple scattering in the walls of the channel, some particles reach the emulsion that have been accepted from outside the geometrically defined acceptance limits. Such particles, however, lose energy in penetration of the wall material and are, therefore, not likely to be found in the neighborhood of the range cutoff of the bias curve[29]. An estimate of this effect is developed in the Appendix (Sec. IX), together with some supporting experimental evidence.

The detector system, or array of detector units, is adjusted (Sec. III, C, 4) so that each unit in the array receives particles leaving the target at the same angle Φ. The particles received in each unit of the array then differ only in momentum, or more properly, $H\rho$. The set of data obtained by track count (Sec. III, C, 6) in the nuclear emulsions of all units in the array constitutes, therefore, a momentum spectrum of the deuterons leaving the target at this angle (Fig. 8). The difference spectrum between the deuterated paraffin and polyethylene targets exhibits a rough spectrum of the incident protons as weighted by the scattering cross section and the acceptance function ΔV (Sec. III, C, 3), and as transformed in momentum through the relation $K = 4/3\, k \cos\Phi$.

These spectra are used to compute the mean energy of the incident protons as shown in Section V.

(2) Nuclear Absorption Loss

The slit scattering problem requires the actual scanning to be done at a point as close as possible to the range cut-off. It is well known, however, that not all particles in an incident flux of a given energy survive the whole distance of their range in matter. Particle loss is due largely to the occurrence of nuclear encounters and the effect is termed nuclear absorption. The evaluation of nuclear absorption loss is accomplished in an auxiliary experiment performed in a 110 Mev external deuteron beam of the cyclotron. The well collimated beam is caused to pass through the copper wedge into a sensitive nuclear plate. The slope of the resulting bias curve, uncomplicated by the effect of slit scattering, is then regarded as a measure of the absorption effect. A correction factor for zero absorber thickness is obtained directly from the ratio of intensity at zero absorber to that at range cut-off. Refer to Fig. 7(b).

It should be pointed out that the form of this bias curve contains, in addition to nuclear absorption, a change in the effective swath width scanned near the range cut-off. This change in brought about by angular straggling of the particles passing through great absorber thicknesses and results from the cumulative effects of small angle multiple scattering. This change in swath width will be made more clear when the factors defining the effective swath width are understood (Sec. III, C, 6). The change in width, however, is automatically taken into account by applying the correction factor for zero absorber thickness and does not require separate treatment.

(3) Particle Acceptance

The basic geometrical acceptance limits or detection function defined by the channel are first calculated neglecting such effects as: (a) the radial decrease of the magnetic field with its attendant radial and vertical focusing effects; (b) the curvature of the particle path in the channel; (c) the effects of slit scattering. To this acceptance function are applied the above three effects in the form of corrections. The result forms a basis for the computation of the solid angle subtended by the detector system at the target.

It is seen, with reference to Fig. 9, that the loci of centers of curvature of all limiting orbits that originate in the target and pass freely through the detector channel enclose a region of space whose volume is readily computed from the geometry. This small volume element may be expressed as:

$$\Delta V = \frac{a^2 z}{b} \frac{\rho}{\sin^2 \frac{\psi}{2}} \qquad (10)$$

neglecting terms of the order $\left(\frac{a}{b}\right)^2$ and higher. In this expression, a, b are the half-width and half-length, respectively, of the channel; ρ is the radius of curvature of the central orbit; and ψ the magnetic field deflection angle. This expression for ΔV is derived in the Appendix (Sec. IX). The use of this volume element, corrected as in Section III, C, 5, will become apparent in Section V, C dealing with the evaluation of the absolute cross section. The height Z is defined in Sec. III, C, 6.

(4) Alignment Technique

The channel of a detector unit is actually constructed in two

short separated sections, articulated to conform as closely as possible to the orbit curvature (Fig. 6). Alignment of the channel is specified by r, the position of its midpoint on the detector probe axis, by α, its orientation relative to this axis, and in addition, orientation angles for the channel segments as determined by the particle radius of curvature. It may be shown that the angle α changes by so little in passing from one channel to the next that negligible error is introduced by actually constructing the channels in units of six, as shown in Fig. 10. It is seen that there are six such units each containing six channels making a total of 36 channels. By convention, the fourth channel in each unit of six is used in alignment. The channel is conveniently and rapidly adjusted to the above specifications by the use of an alignment template, a point source of light, and a pair of mirrors (Fig. 11). The template consists of a large protractor on which the detector system is clamped, connected by a rigid beam to a drawing board on which are plotted the coordinates of the centers of curvature of the orbits to be accepted. The light source is placed on the desired coordinate which is a distance ρ from the channel. The mirrors clamped with their glass surfaces parallel to the channel walls, return the light from the source to a screen located directly above the source. By masking the mirror surface so as to expose only a narrow slit located at the midpoint of the channel segment, the slit images of both mirrors may be accurately adjusted to coincide with a mark on the screen located over the coordinate. When this is done, the channel segments are perpendicular to the radius of curvature and hence tangent to the orbit. The practical limit of error in this adjustment is of the order of magnitude of one minute of arc. The coordinate r has

an associated error of the order of 0.3%. The average time required to carry out this adjustment on all six units is about 15 minutes, not including the time required to remove and replace the detector system in the vacuum tank of the cyclotron.

(5) Corrections for Particle Acceptance

a. The radial decrease in that portion of the magnetic field utilized in this experiment for momentum analysis amounts to about 2%, falling off very nearly linearly with radius. We adopt here the perturbation point of view in calculating the effect on ion orbits and corrections to the acceptance volume element ΔV.

The radial perturbation is estimated by a graphical method due to Parkins and Critenden[32], in which the motion of the center of curvature is followed graphically. The particle coordinates r, θ at the ends of successive arcs is computed as the motion is followed. Since it is the small change $\Delta\rho$ rather than ρ itself that is plotted, the method possesses considerable advantages over the conventional method of plotting the orbit directly. The results of this analysis show that the orbit is shifted outward by the order of magnitude of 2%. The ρ of particles actually received is, therefore, reduced by this amount. The method is, however, rather time consuming and since the correction is small, it is felt that the calculation of sufficient cases to apply the correction is not justified. This correction, which would tend to reduce the cross section by 2%, is therefore neglected.

The vertical perturbation tending to produce a focusing effect is of more serious consequence than the above. We treat the perturbation

as in the case of free vertical oscillations since the amplitude is necessarily small. The frequency of such oscillations is $\sqrt{n}\omega_o$ [26] where n is generally evaluated at the unperturbed orbit radius. In this case, however, the orbits are considerably off-center. On the other hand, we are concerned only with a small part of the period of motion. We use a weighted mean value, $\overline{\sqrt{n}}$,averaged over the ion paths between target and detector:

$$\overline{\sqrt{n}} = \frac{\int_0^{S=\rho\psi} \sqrt{n}\,(S-s)\,ds}{\int_0^{S} (S-s)\,ds}$$

The fractional increase to the vertical extent Z of Δ V due to this focus effect is:

$$\frac{\Delta z}{z} = 2\left(\sqrt{n}\,\psi - \sin\sqrt{n}\,\psi\right)$$

and the cross sections are reduced by the factor F_z:

$$F_z = 1 - \frac{\Delta z}{z}$$

The factor $\frac{\Delta z}{z}$ is listed in Table II.

TABLE II

Vertical Focus Correction

Target Radius	-10°	-5°	0°	5°	10°	15°	20°
42.0"			.031	.042	.055	.075	.094
45.5"		.025	.038	.051	.067	.088	.110
49.5"	.021	.030	.046				

b. The orbit curvature in the channel effectively reduces the value of the half-width by an amount δa. Since ΔV is proportional to a^2, the correction for ΔV is of the form:

$$\Delta V' = \Delta V = \left(1 - \frac{2\delta a}{a}\right)$$

We have a chord of length $\frac{2b}{3}$ in an arc of radius ρ. δa is then $\frac{b^2}{18\rho}$ and for $2b = 9.85$ cm, $2a = 0.318$ cm, a typical value of $\rho = 150$ cm, the correction increases the cross section by 1.11%.

c. Since slit scattering is accompanied by energy loss, the effect of slit scattering is to enlarge ΔV by an amount that depends on the energy discrimination of the detector. Thus slit scattering increases the slope of the bias curve over that already produced by the effect of nuclear absorption loss. We estimate the contribution of slit scattering at the operating point on the bias curve, namely, the point at which the scanning is done, 0.05 cm of residual range. E.D. Courant[29] has considered this problem using diffusion theory and the statistics of small angle multiple scattering. As is shown in the Appendix, Sec. IX, the effective increase of ΔV on this account is about 4.4% hence the cross section is depressed by this amount.

(6) Method of Scanning

An understanding of the method of scanning the nuclear plates is facilitated by reference to a photographic reproduction of a set of nuclear plates (Fig. 12). These particular plates were obtained by "over exposure" in a large flux of deuterons and tritons produced in

a carbon target into the angle $\Phi = 0^{\circ}$. For this purpose, the proton beam was unrestricted by vertical aperture clipping. Otherwise, the exposure was normal and thus illustrates in a rough way the performance of the detector system. At each channel location a portion of the emulsion is not covered by the copper absorber and is exposed to light which produces a heavy black image on the emulsion surface serving to locate the knife edge of the absorber wedge. Below this fiducial mark a grey rectangular region is seen, containing in this case far too many tracks for reliable counting. The grey region is terminated rather abruptly at a point corresponding to the range cut-off of deuterons. A second cut-off may be seen emerging from the diminishing deuteron background in the third and fourth plates. This second cut-off is clearly due to tritons since the range is about one-third that of the deuterons. It may be further noted that besides the gradual increase in range with r, there is a perceptible increase in range within each channel, also with increasing r. Both effects are to be expected from the geometry and constitute internal checks for the alignment of the detector system.

For two reasons the scanning is done at fixed distance short of the range cut-off: (1) the grain density in a track is proportional to the energy loss as is well known. The nuclear emulsions used, Ilford C-2, are of insufficient sensitivity to permit reliable track count of swift particles, let us say $>$ 30 Mev deuterons. Experiments using plates sensitive to minimum ionizing particles were nearly clogged with electron tracks resulting from the high level gamma ray background in the cyclotron; (2) to rid the track count as much as possible of the unwanted particles accepted by the slit scattering, it is necessary to

work as close as possible to the cut-off of the bias curve (See Sec. III, C, 5). The point arbitrarily chosen is 0.5 mm from the mean range cut-off. The scanned swath extends from well outside the track locus on one side to well outside it on the other (1.0 mm on either side).

The tracks dive through the unprocesses emulsion at the 45° angle determined by the copper wedge. After processing the emulsion shrinks about 50% in thickness while the lateral shrinkage is negligible. Therefore, the tracks show a dip angle of about 27° in the processed emulsion under a microscope. Under an oil immersion objective of 95 x the depth of focus is so short that only a small portion of the track is visible at one time, although it actually extends over three fourths of a field of view. Racking the fine-focus adjustment up and down produces an effect in which the short visible section of track appears to move back and forth along its length. These tracks are roughly parallel to the Y-axis of the field of view. An eye-piece reticle is used to project a fine horizontal X-axis line onto the object plane.

Criteria for the acceptance of tracks permit easy and rapid recognition. (1) The track must "move" in the right sense with the fine-focus racking motion and the "velocity" must be judged to be within a factor of two of a track measuring a 27° dip angle. (2) The track must be straight and fall within an angle of 45° to the Y-axis. (3) the track must intersect the X-axis (reticle) line at some point along its length. (4) The track must enter through the top surface of the emulsion. Items (1) and (2) are particularly easy to apply in most cases as there are, typically, many characteristic tracks in a field of view all at once for convenient comparison. Item (4) is not strictly enforced but is

generally applied to obvious cases when the track is seen to begin within the body of emulsion. Such tracks are attributed to proton recoils due to neutron background.

It should be noted that Item (3) defines the effective width of the swath. The quantity Z, entering in the calculation of the volume element ΔV (Sec. III, C, 3, above) is evidently the product of the number of swaths taken, the thickness of the unprocessed emulsion, and tangent of the slope angle, 45°, of the copper wedge. The effect of angle straggling, requiring angular limits for track acceptance is specifically excluded from the determination of Z as it is included implicitly in the correction factor for zero absorber thickness.

The scanning is done in a continuous motion. The motion of the mechanical stage in the X-direction is driven by a variable speed motor. At the same time, the fine-focus adjustment is racked up and down manually at a suitable rate so as not to miss any tracks meeting the acceptance criteria. The track count is tallied on a hand register and recorded at the completion of a swath. Generally, three such swaths are made, separated in the Y-direction just sufficiently to avoid counting the same tracks twice. This is done both as a control measure, the three counts should agree within the probable error, and as an efficient method for gaining greater counting statistics. A scanner experienced in this technique can complete one channel in about ten minutes, frequently counting at rates exceeding eighty a minute.

It should be mentioned that background tracks meeting the acceptance criteria tend to cancel out in making the subtraction between the results of the two targets. To check on this point, the background may be estimated by scanning swaths located just beyond the range cut-off.

IV. DETAILS OF APPARATUS

A. Beam Clipper and Target Support

The beam clipper and target support mechanism are shown in Fig. 13. Since the primary function of the clipper is to limit multiple passage of the beam through the target, aperture limits are required both above and below the beam. It was found necessary to employ four independently adjustable jaws for this purpose in order to accommodate irregularities in the magnet median plane. With this device it has been found possible to bring the beam out through its effective eight inches at an aperture of one-eighth inch in each pair of jaws. Ordinarily, the copper fin is adjusted so that the resulting beam is slightly greater than $\frac{1}{4}$ inch at the entrance end of the clipper. After carefully leveling the device, the pair of jaws at the entrance end is adjusted to trim this beam to $\frac{1}{4}$ inch. The second pair are then adjusted to just graze this beam emerging from the first. All these adjustments are greatly facilitated by the use of thin pieces of glass which are blackened by the passage of protons. Finally, the targets are mounted in the sliding carrier and adjusted by limit stops so that only the target material itself is exposed to the beam. The first target, say CD_2, is run with the carrier in the position shown, held in place by a spring loaded catch. To substitute the CH_2 target current is passed through a flip coil, visible between the pairs of clipper jaws, which trips the catch allowing the carrier to drop into the second target position. The operation of the target changer is viewed through a port hole in the cyclotron vacuum tank to make certain of its proper operation.

(1) Targets

The targets are mounted in brass holders which fit into the support carrier. The holders themselves are shielded from the primary beam by the clipper. The deuterium paraffin has a density 1.0501 gm cm^{-3} and contains 97% deuterium, according to the analysis supplied with the sample prepared by the Texas Company. As prepared in the target form used it has an aereal density of 0.3098 gm cm^{-2}. The polyethelene target has an aereal density of 0.2870 gm cm^{-2}. Thus the molar ratio of CD_2 to CH_2 in the two targets is 0.947 and the stopping power and multiple scattering factors in the two targets are matched to within 5%. The stopping power of the CH_2 target is 1.78 Mev for 130 Mev protons, and is 1.69 Mev in the CD_2 target. The 0.09 Mev discrepancy produces a difference of 0.03% in radius of curvature in the two cases and is considered negligible.

B. Monitor System

As indicated above, (Sec. III, B) the activity in the targets is determined by the use of an ionization chamber sensitive only to the annihilation radiation resulting from the C^{11} positron emission. The charge, resulting from the ionization current is collected on a cylindrical brass condenser of 3 cm capacity.

The condenser plate to which the charge is transferred is connected to the gilded quartz fiber suspension of a Ryerson-Lindemann quadrant electrometer[30]. The collection of charge on the condenser plate raises its potential relative to ground, producing a deflection of the quartz fiber. This fiber may be returned to the zero deflection

position by the application of a negative voltage on the opposite condenser plate. In practice, the deflection is kept small by continuously raising the applied voltage, in proportion to the charge collected. The reciprocal of the time required for a null deflection at a specified applied voltage constitutes a measure of the activity.

C. Detector System

The actual construction of the detector array is illustrated in Fig. 10. Each six-channel unit is milled out of a single block of brass. The channel segments are 0.1250 ± 0.0005 inch in width, 1.063 ± 0.001 length, 1 inch top to bottom. The hole for the articulation clamping screw is located and machined before the two halves of the unit are separated by a $\frac{1}{4}$ inch cut. This procedure assures the proper relative alignment of the two sections of the articulated channel. In the photograph, one of the baffle systems, used to prevent cross-fire between channels, is removed to show the clamping screw and the method of articulation. The copper wedges and lands provided to locate the nuclear plates terminate the channels. The whole assembly is introduced through an air lock into the vacuum system of the cyclotron where it slides along ways located (as in Fig. 1) on a radius line $154^{\circ}40'$ in azimuth from the target radius.

(1) Alignment Template

The alignment template is an important auxiliary to the detector system. Its construction and use are illustrated in Figs. 11, 14. On the coordinate board are plotted the centers of curvature of orbits entering the fourth channel in each six channel unit. The calculations of these coordinates are based on the circular orbit (uniform field)

approximation, in which the center of curvature is fixed in the horizontal plane. The effect of the radial decrease in the field shifts the final location of the center of curvature by the order of magnitude 2% (Sec. III, C, 5) but this effect is neglected.

V. ANALYSIS OF DATA

A. Monitor

Decay curves are run on each target and the activity A referred to the time of ending the bombardment is computed on the basis of the best value of the half life of C^{11}; $t_{\frac{1}{2}} = 20.5$ minutes. This value which agrees with that quoted by Siegbahn[27] was obtained from a detailed analysis of the decay curves obtained in the Linear Accelerator calibration runs mentioned in Sec. III, B. The detailed procedure is also applied in many cases in actual runs: (1) to obtain from the data the best value of A_o and the associated probable error, (2) to detect, through similar trends in the A_{oi}, the presence of possible contamination activities due, for example, to the inadvertant activation of the brass target holder through misalignment of the target support.

The monitor quantity $\frac{2NQ}{e}$ is given as in (8) of Sec. III, B:

$$\frac{2NQ}{e} = \frac{2K_o A_D}{\sigma_{ppn(E)}} \frac{\lambda t_D}{1-e^{-\lambda t_D}} \tag{11}$$

where A_D is the activity of the deuterated target at the end of a bombardment of duration t_D, but the p,pn cross section is now averaged over the incident proton spectrum. A method leading to an evaluation of $\overline{\sigma_{ppn}}$ is indicated in the next section.

From the polyethylene target similar data are obtained. The ratio of both sets of monitor data

$$S_M = \left(\frac{A_D}{A_H}\right)\left(\frac{t_D}{t_H}\right)\left(\frac{1-e^{-\lambda t_H}}{1-e^{-\lambda t_D}}\right) \tag{12}$$

is used in obtaining the net yield from deuterium in the deuterated target.

The monitor calibration experiment essentially follows the procedure at 31 Mev of Reference (28), using the same Faraday cup. The chief difference in this case is the use of 1 Mev thick targets of polyethylene and the use of the ionization chamber in place of a calibrated β-counter. Seven runs were made giving:

$$K_o = (1.354 \pm 0.009)\ 10^9$$

B. Detector

The point at which the scanning is to be done is first located, the initial point being marked with a microscope attachment. The procedure followed also yields the range in copper of the detected particle for use as an internal check on the alignment. The marked plates are then scanned as in Sec. III, C, 6, and the results tabulated. The difference

$$D_i = C_{Di} - S_m C_{Hi} \qquad (13)$$

is the yield from deuterium into the narrow range of momenta about a central value determined by the position and orientation of the i^{th} channel. The set of D_i for all the channels constitutes a momentum spectrum of the elastic recoil deuterons. From this spectrum a mean value of the incident proton energy is inferred and used to determine an appropriate value of $\overline{\sigma_{p,pn}(E)}$ from the data of Reference (28).

The nuclear absorption loss experiment mentioned in Section III, C, 2 involves the use of a well collimated externally deflected beam of deuterons degraded in energy to 110 Mev by an absorber placed in the cyclotron at the exit end of the magnetic deflection channel. The energy

straggling produced by the absorber is believed partly reduced by magnetically focusing the beam through the collimator.

Two exposures in the 1/8 inch wide, 1 inch high emerging beam are made in the same plate, one through a copper wedge, the other with the copper wedge moved out of the beam in one direction and the plate moved in the opposite direction. Thus at each Y-coordinate the track count in the two exposures give, respectively, a transmission and a monitor value. The ratios are plotted against the Y-coordinate in Fig. 7(b) where Y = 0 at zero copper thickness. The slope seems to represent a mean absorption cross section for deuterons of 4.05 barns which is perhaps not unreasonable. On the basis of this curve, the correction A for nuclear absorption loss is obtained as follows: .17 ± 0.06, .23 ± 0.07, and .28 ± 0.09 for experiments at mean proton energies of 95, 112, 138 Mev, respectively.

It should be remarked that in all cases the fourth channel in each six channel unit is scanned, and in some cases, to give added statistical weight as well as improved definition of the incident proton spectrum, channels 2 and 6 were also scanned.

C. Absolute Cross Section

Consider what limitations the acceptance volume element ΔV imposes on the momentum $\vec{K}$ a particle leaving the target. It is convenient here to define a momentum $\vec{P}$ in units of length by the radius of curvature ρ :

$$\vec{P} = \frac{\rho}{|\vec{K}_\perp|} \vec{K}_\perp \qquad (14)$$

Motion parallel to the field $\vec{K}_{\parallel}$ is negligibly small for the detected particles so that we may consider $\vec{K}_{\perp} = \vec{K}$. Evidently the magnitude and Φ-direction of $\vec{P}$ are bounded in precisely the same way as the length and direction of the extension of ρ from the target. The dip angle of $\vec{P}$ is just Z/S where $S = \rho\psi$ is the path length from target to detector. The limit on the momentum $\vec{P}$ is thus essentially a prism shaped region of the same base as ΔV but with height:

$$\frac{P z}{\rho \psi} = \frac{z}{\psi}$$

The region $\Delta V/\psi$ limiting $\vec{P}$ imposes the following limits:

$$\frac{\Delta P}{P} = \frac{\Delta P}{P}(\Phi) \approx \frac{a}{\rho} \sin\frac{\psi}{2} \approx 2(10)^{-3}$$

$$\Delta\Phi = \frac{a}{c} \sin\frac{\psi}{2} \approx \frac{a}{c} = .0322$$

$$\frac{z}{\rho\psi} \approx 2(10)^{-5}$$

The yield of recoil deuterons, D_i in the $i^{\underline{th}}$ channel is

$$D_i = 2N t_D \int dE \int d\Omega(E)\, I(E)\, \frac{d\sigma(\Phi, E)}{d\Omega} \qquad (15)$$

where: $I(E)$ = flux of protons per unit time per unit energy

t_D = duration of bombardment

$\frac{d\sigma(\Phi E)}{d\Omega}$ = differential cross section a function of E, and the integration is to be performed subject to the limits imposed by $\Delta V/\psi$.

We introduce a relation between the incident energy and the recoil deuteron momentum, but supress the angular dependence in view of the magnitude of $\Delta\Phi$ by evaluating it at the average value of Φ in $\Delta V/\psi$ thus:

$$E = F(P, \Phi) = F(P)$$

$$dE = \frac{dF}{dP} dP$$

Also, since the integrand, which now becomes $I(P)\left(\frac{dF}{dP}\right)\left(\frac{d\sigma}{d\Omega}\right)$, varies negligibly over the limits of $\Delta V/\psi$ we take it as constant and are left with the integral:

$$\iint_{\Delta V/\psi} dP\,d\Omega = \int_{P_{min}}^{P_{max}} dP \int_{\Delta\Omega(P)} d\Omega = \int_{P_{min}}^{P_{max}} \frac{A(P)}{P^2}\,dP$$

Where A(P) is the area of a section of the acceptance volume by a plane perpendicular to P. P^2 is certainly slow varying in the denominator compared to A(P) in view of the magnitude of $\Delta P/P$.

The result of the integration is then obviously $\frac{\Delta V}{P^2\psi}$, and the yield becomes:

$$D_i = 2NI(P_i)\left(\frac{dF}{dP}\right)_i \frac{d\sigma}{d\Omega}\frac{\Delta V_i}{P_i^2\psi_i}$$

The yield per unit solid angle per unit momentum into the $i^{\underline{th}}$ channel is

$$\frac{D_i\psi_i P_i^2}{\Delta V_i} = 2NI(P_i)\left(\frac{dF}{dP}\right)_i \frac{d\sigma}{d\Omega} \tag{16}$$

and the total yield per unit solid angle is got by summing over the channels, and integrating over the momentum or energy spectrum.

$$\sum_i \frac{D_i\psi_i P_i^2 \Delta P_i}{\Delta V_i} = 2N\int_0^\infty I(P)\frac{dF}{dP}\frac{d\sigma}{d\Omega}\,dP = 2N\int_0^\infty I(E)\frac{d\sigma}{d\Omega}\,dE \tag{17}$$

Where ΔP_i is the separation in P between the i and $(i+1)^{\underline{st}}$ channel.

The yield of C^{11} is

$$Y = K_0 A_D = N_0 \overline{\sigma_{pn}(E)} \left(\frac{1-e^{-\lambda t_0}}{\lambda t_0}\right)\int_0^\infty I(E)\,dE \tag{18}$$

in which we have made use of the form of the deuteron yield spectrum to infer an appropriate mean value of $\overline{\sigma_{pp}(E)}$. It is found that the variation in σ over the extent of I(E) is of the order of 5%.

Dividing (17) by (18) and making use of (11) and (14) we have

$$\left(\frac{1}{\frac{2NQ}{e}}\right)\sum \frac{D_i \Psi_i \rho_i^2 \Delta\rho_i}{\Delta V_i} = \frac{\int_0^\infty I(E)\left(\frac{d\sigma(\Phi,E)}{d\Omega}\right)dE}{\int_0^\infty I(E)\,dE} \qquad (19)$$

which is evidently the differential cross section averaged over the incident spectrum.

Because of corrections indicated in previous sections, the cross section is:

$$\frac{d\overline{\sigma(\Phi)}^{\epsilon}}{d\Omega} = \frac{F}{\left(\frac{2N_0Q}{e}\right)}\sum \frac{D_i \Psi_i \rho_i^2 \Delta\rho_i}{\Delta V_i}$$

Where F contains the following:

A = nuclear absorption loss. Sections III, C, 2; V, B

B = magnetic field non-uniformity. Section III, C, 5; Table II

C = orbit curvature in channel. Section III, C, 5

S = slit scattering. Section III, C, 5 and Appendix B

F = (1 + A - B + C - S)

The factor F is listed in Table III, Section VI.

The transformation of $d\sigma/d\Omega$ from the deuteron angle Φ in the laboratory system to the proton angle θ in the center of mass system may be understood with reference to Fig. 15(a). It will be seen that

$$\frac{2}{3}k\sin(\pi-\theta) = \frac{4}{3}k\sin\Phi\cos\Phi$$

or

$$\sin(\pi-\Theta) = \sin 2\Phi$$

so that

$$\Theta = \pi - 2\Phi$$

and

$$\frac{d\cos\Phi}{d\cos\Theta} = \frac{\sin\Phi}{2\sin 2\Phi}$$

so, the cross section becomes

$$\frac{d\sigma(\Theta)}{d\Omega} = \frac{\sin\Phi}{2\sin 2\Phi}\,\frac{d\sigma(\Phi)}{d\Omega} \qquad (20)$$

D. Sample Calculations

(1) Calibration constant, run Number 6. From (7):

$$K_o = \frac{NQ(t)}{e}\,\frac{\sigma_{pp}(E)}{A(t)}$$

with

No = 6.02 (10)^{23} atoms mol^{-1}

M = 14.071 gm mol^{-1} (CH_2)

e = 1.602 (10)$^{-19}$ coulomb

E = 32 Mev

σ = 89 (10)$^{-27}$ cm^2

ρ_A = 0.0710 gm cm^{-2}

we have

$$\frac{N\sigma}{e} = 1.691(10)^{15}$$

and experimentally with C = 9.94 μf:

$$A(t_o) = 4.09 \text{ (integrator decavolt) (min)}^{-1}$$

$$Q(t_o) = 3.302\ (10)^{-6} \text{ coulombs} = C\,V = (9.94\,\mu f)(0.332 \text{ volt})$$

hence

$$K_o = 1.365\ (10)^{9} \text{(minutes)(integrator decavolt)}^{-1}$$

(2) Differential cross section. Item 4, Table III, Sec. VI.

$$A_D = 15.5 \text{ (integrator decavolt)(min)}^{-1}$$

$$A_H = 20.0$$

$$t_D = 10.01 \text{ min}$$

$$t_H = 10.00 \text{ min}$$

$\therefore$ from Equation (12): S = 0.775

$$\Sigma C_{Di} = 969 \text{ tracks}$$

$$\Sigma C_{Hi} = 643$$

$$\therefore \quad \Sigma D_i = 969 - (0.775)\ 643 = 470.7 \pm 37$$

The mean energy as estimated from the spectrum is 98 Mev. The corresponding $\sigma_{p,pn} = 70.5\ (10)^{-27}$ cm^2. The target radius was 42 inches, the detector set for $\Phi = 0$ so that

$$\psi \sin^2\frac{\psi}{2}\,\rho\,\Delta\rho = 218.0$$

with a = 0.0625, b = 1.938, Z = 0.00417 inch, F = 1.111, and $d(\cos\Phi)/d(\cos\theta) = 0.250$, we have

$$\frac{d\sigma(180^\circ)}{d\Omega} = \frac{F}{\left(\frac{2NQ}{e}\right)}\left(\Sigma D_i\right)\left(\frac{\psi\rho^2\Delta\rho}{\Delta V}\right)\frac{d\cos\Phi}{d\cos\theta} = (4.80 \pm 0.38)(10)^{-27}$$

VI. PRESENTATION OF DATA

The cross sections measured in this experiment are shown in Table III and IV, and Figs. 16 and 17. The indicated errors include only the statistical standard deviations associated with the track counts. It is evident that there is present some experimental error. If it is assumed that the error is random in nature, then it appears, from an analysis of the absolute yield of the deuterated and polethylene targets that items 2, 3, 5, 7, 9, and 10 of Table II, all taken on one day, show much greater lack of control then the rest. In Table IV and Fig. 17, average values of the cross sections are presented in which the data were combined giving items 2, 3, 5, and 7 a weight 1/3 relative to the rest. Actually this weighting procedure makes very little difference in the results shown. Analysis of the Range-ρ relationship, and monitor decay curves show no evidence of gross misalignment of the apparatus. The scanning procedure was carefully checked for reliability by having different observers determine independent cross sections from the same set of plates. The results check within probable error. In addition, different observers were required to scan independently the same five swaths as a direct test and the results agreed within 2%.

The errors associated with the absolute value assignment to the cross section are as follows:

(1)	C^{11} excitation function calibration	11%
	F factor correction estimate	8.5%
	Scanning	2%
	Root mean square total	13.8%

(2) The apparent experimental error evident from reproducibility is believed to be of the order of 25% if the weight 1/3 is given the points mentioned above. This is much larger than the counting statistics which are of the order of 8%. Some justification for the assumption that the experimental errors are random is attempted in the discussion of the results, Sec. VII.

TABLE III

Differential Scattering Cross Section

Differential scattering cross section $d\sigma(\theta)/d\Omega$, millibarns per steradian in center of mass system as a function of the center of mass angle θ degrees. Also shown are the cyclotron target radius r_T inches, the mean incident proton energy E Mev the observation angle Φ degrees, and in the second column, the correction factor F which has been applied. The error shown is the standard deviation.

Item	F	r_T	E	Φ	θ	$d\sigma(\theta)/d\Omega$	$\pm\Delta(d\sigma/d\Omega)$
1	1.11	42	95	0	180	4.81	0.42
2						3.61	0.18
3						5.79	0.33
4						4.80	0.38
5	1.091			5	170	4.12	0.37
6						2.10	0.12
7	1.072			10	160	1.24	0.14
8						1.55	0.24
9	1.055			15	150	1.98	0.38
10	1.047			20	140	0.97	0.21
11	1.110	45.5	112	0	180	3.32	0.13
12						3.38	0.29
13	1.095			5	170	2.48	0.34
14	1.112			-5	170	1.65	0.36
15	1.078			10	160	0.575	0.238

TABLE III (cont)

Item	F	r_T	E	Φ	θ	$d\sigma(\theta)/d\Omega$	$\pm\Delta(d\sigma/d\Omega)$
16						1.72	0.24
17						1.06	0.29
18	1.059			15	150	1.10	0.19
19						0.83	0.13
20	1.048			20	140	0.87	0.20
21	1.060	49.5	138	0	180	2.10	0.21
22						1.54	0.24
23	1.078			-5	170	1.18	0.21
24	1.089			-10	160	0.54	0.06

TABLE IV

Weighted Average Differential Cross Section

Weighted average values of differential cross section $d\sigma(\theta)/d\Omega$, millibarns per steradian in center of mass system as a function of center of mass angle θ degrees. The error shown is the standard deviation.

E Mev	140°	150°	160°	170°	180°
95	0.97 ± 0.21	1.98 ± 0.38	1.47 ± 0.21	2.62 ± 0.14	4.78 ± 0.43
112	0.87 ± 0.20	0.97 ± 0.21	1.12 ± 0.26	2.06 ± 0.35	3.35 ± 0.23
138			0.54 ± 0.06	1.18 ± 0.21	1.82 ± 0.23

VII. DISCUSSION OF RESULTS

Two facts seem to have emerged as a result of this experiment. The one has to do with the pick-up process in proton deuteron scattering, the principal objective of this study. The other has to do with some properties of the 184 inch Berkeley synchrocyclotron. Since these cyclotron properties are of perhaps less general interest, let us touch on them briefly and then return to the principal subject.

It was emphasized in Sec. III that the spread in energy incident on an internal cyclotron target requires consideration in an experiment of this kind; that radial oscillations in the circulating beam are known to be present. Figure 3 shows what we believe to be a representation of the energy spread at a target radius of 42" where the expected proton energy, 110 Mev, is shown in dotted line. The shape, half-width, and displacement of peak is very similar to that obtained in the Harvard synchrocyclotron[33]. The displacement of the peak, about 15 Mev, represents a mean radial oscillation amplitude of $3\frac{1}{2}$ to 4 inches at this radius. Actually, the deuteron spectra from which this information is obtained show a shift in peak energy from one day to the next and the average is about 3 inches. Note that there are few unperturbed ions present. In the perturbed motion, the action

$$\sqrt{n}(\Delta z)^2 + \sqrt{1-n}(\Delta r)^2 = \text{constant}$$

for the adiabatic transfer of the orbit to the exit radius. The change in n is from 0.029 at 42 inches to 0.113 at 80 inches. Now $\Delta Z/\Delta r \sim 0.1$ so that neglecting ΔZ compared to Δr it is clear that Δr will be practically unchanged at 80 inches so that the mean energy on an internal

target at 80-3/4 inches is likely to be 320 rather than 340 Mev as expected. Moreover, the full width at half maximum would be 20 Mev on this basis.

Let us now return to the principal objective of the experiment. The solid curve of Fig. 17 is the prediction of Chew[15] for neutron deuteron elastic scattering into the region of large angles. According to the theory, the peak is essentially due to the pick-up process sketched in Sec. I. It was shown there that the cross section is proportional to the fourth power of the Fourier component of the deuteron wave function corresponding to the momentum, $\vec{R}-\vec{k}$. Owing to the circumstance that $|\vec{R}-\vec{k}| = |\vec{k}-\vec{R}/2|$, Equation (4), it follows that

$$E_p = \frac{|\vec{R}-\vec{k}|^2}{2m} = E\left(1-\frac{2}{9}\cos^2\Phi\right) \qquad (21)$$

is the energy of the proton left behind. We may regard the cross section as being a function of E_p alone, apart from a weak purely angular dependence in addition to this. Thus, (21) can be used to predict the energy and angular distribution at another energy if it is known at one. Figure 15(b) shows a diagram for the vectors involved.

As mentioned in Sec. VI, the point of view was taken that the apparent experimental errors of certain points at 95 Mev were more or less random in nature. This assumption was based on the fact that for the three sets of data the effect of (21) was quite apparent and all three sets of data could be compared on this basis.

The long dashed curve of Fig. 17 at 95 Mev represents Chew's curve multiplied by the factor 0.55. The dashed curves through the 112 and 138 Mev data are obtained from it by the relation (21). The agreement

seems to be satisfactory.

The data of Powell[20] is not inconsistent with the long dashed curve at 95 Mev. The short dashed curve represents a curve taken from the paper by Stern[19] which had been passed through the experimental points to 170° and extrapolated to 180°.

It might be said that over the limited energy range explored in this experiment, the cross section is in agreement with the characteristic behavior of the pick-up process. However the magnitude of the cross section is lower than predicted and it may be that the fault lies in the use of the Born approximation or that there may be present in the process a more direct influence on the cross section of the third particle present[31].

VIII. ACKNOWLEDGMENTS

The author wishes to thank Professor Burton J. Moyer for continued interest and stimulating encouragement in this work, and Professor Owen Chamberlain for some very valuable suggestions. He is indebted to Mr. Charles Godfrey and Mr. Jerome Kaplan for the tedious range measurements. He is most deeply in debt and grateful for the patience of those observers who managed to count altogether more than $5(10)^4$ tracks: Mr. Roland Michaelis, Mrs. Edith A. Goodwin, Miss Irma Sturgill, and Miss Mary Lee Griswold. To Mr. James Vale and the cyclotron crew he is particularly indebted for their splendid cooperation in an experiment that required an unusual amount of manipulation and fine adjustment.

This work was performed under the auspices of the Atomic Energy Commission.

IX. APPENDIX

A. The Acceptance Volume Element ΔV

Figure 9 shows schematically the geometry involved in computing ΔV. The base of the prism containing all centers of curvature accepted by the channel has an area

$$A = \frac{\rho_1 + \rho_2}{2} \frac{a}{b} W$$

When ρ_1, ρ_2 are the radii of curvature at the extreme acceptance angles and W is the width of this area measured along ρ. Evidently $\frac{\rho_1+\rho_2}{2} = \rho$.

$$\Delta\rho = 2a - W$$

Now for $\Delta\rho \ll \rho$, $\Delta\rho = W \cos 2\beta$ where β is the angle between ρ and the line forming channel and target. Since $2\beta = \psi - \pi$,

$$W = \frac{2a}{1+\cos 2\beta} = \frac{a}{\sin^2 \psi/2}$$

The orbit in uniform field approximation is a spiral and the vertical motion of the center of curvature is limited by Z the height of the detector, Fig. 9(b), hence:

$$\Delta V = \frac{a^2 z}{b} \frac{\rho}{\sin^2 \psi/2} \qquad (10)$$

B. Slit Scattering

With the channel geometry used here, two types of multiple small angle scattering processes appear. (1) Particles strike front

face and scatter through a corner into the channel and possibly out through diagonally opposite rear corner, (2) particles are "reflected" from inside wall. Here one also considers single Rutherford scattering contribution with little or no energy loss.

As an estimate of type (1), Courant[29] gives a formula for the effective increase in slit width for a beam of particles incident at angle θ, possessing a root mean square scatter angle θ_o, traversing a path length t.

$$D_1 = \frac{1}{\sqrt{3\pi}} \theta_o t \left[e^{-z^2} + \text{erf}\, z \right]$$

with

$$z = \sqrt{\frac{3}{t}} \frac{\theta}{\theta_o}$$

Unfortunately, this formula neglects angular acceptance restrictions beyond the first slit and so seriously overestimates the effect in the particular case at hand. We use this formula for $\theta = 0$, and compute the contribution at larger angles on the basis of straight line paths through the channel wall. For $\theta = 0$ we have

$$D_1(0) = \frac{1}{\sqrt{3\pi}} \theta_o t$$

and with t = 0.05 cm, and θ_o = 0.0188 radian, $D_1(0)$ = 0.00031 cm.

For particles at θ using the straight path approximation in channel of length 2b, width 2a:

$$D_1(\theta) = \begin{cases} 2t \sin\theta \cos\theta \approx 2t\theta & \theta \le \frac{a}{b} \\ 2(t-b)\theta + a & \frac{a}{b} \le \theta \le \theta_{max} \end{cases}$$

$$\theta_{max} = \frac{2a}{2b-t}$$

and for

$2a = 0.318$ cm

$2b = 9.85$ cm

$\frac{a}{t} = 0.0322$ radius

$t = 0.050$ cm

θ_{max} and $D_1(\frac{a}{t}) = 0.00322$. The fractional increase in ΔV, assuming a linear increase of D from $\theta = 0$ is:

$$\frac{\frac{1}{2}\left[D_1\left(\frac{a}{t}\right) + D_1(0)\right]}{a} = \frac{0.0017}{0.16} = 0.0105$$

As an estimate of type (2) we use the formula of Courant

$$D_2 = \frac{1}{2} C \theta (1 - erf z)$$

where C is the length of channel wall exposed to an incident beam at angle θ. The area A under the curve of $D_2(\theta)$ versus θ, obtained by numerical integration is related to the fractional increase in ΔV as follows:

$$\frac{\delta(\Delta V)}{\Delta V} = \frac{AC}{2a^2}$$

For $t = 0.05$, $C = 3.28$ cm, A turns out to be 0.00035 so that

$$\frac{\delta(\Delta V)}{\Delta V} = 0.0334$$

An estimate of single coulomb or Rutherford scattering accompanied by an energy loss equivalent to 0.05 cm turns out to be quite negligible.

The total effective increase in ΔV due to processes of the two types is then $1.1 + 3.3 = 4.4\%$. We take for the scattering correction, $S = 0.044 \pm 0.044$. It is interesting to note that the bias

curve shown in Fig. 7(a) also shows an effect of the same order of magnitude for a residual range of 0.05 cm.

X. REFERENCES

(1) J. Hadley and H. F. York, Phys Rev 80, 345 (1950)

(2) K. Brueckner and W. Powell, Phys Rev 75, 1274 (1949)

(3) H. Bradner, Phys Rev 75, 1467 (1949)

(4) H. A. Bethe, Rev Mod Phys 9, 69 (1937)

(5) G. Chew and M. Goldberger, Phys Rev 77, 470 (1950)

(6) J. Heidmann, Phys Rev 80, 171 (1950)

(7) R. Serber, Phys Rev 72, 1008 (1947)

(8) J. B. Cladis, Thesis, UCRL-1621

(9) P. Wolf, Thesis, UCRL-1410

(10) E. M. Henley and R. H. Huddleston, Phys Rev 82, 854 (1951)

(11) O. Chamberlain and E. Segre, UCRL-1735, to be published Phys Rev

(12) A. Bratenahl, R. H. Hildebrand, C. E. Leith, and B. J. Moyer, Phys Rev 75, 7 (1949)

(13) S. Fernbach, R. Serber, and T. B. Taylor, Phys Rev 75, 1352 (1949)

(14) J. Blatt and J. D. Jackson, Phys Rev 76, 18 (1949)

(15) G. F. Chew, Phys Rev, 74, 809 (1948)

(16) R. L. Gluckstern and H. A. Bethe, Phys Rev 81, 761 (1951)

(17) J. H. Coon and R. F. Taschek, Phys Rev 76, 710 (1949)

(18) J. Hadley, Thesis, UCRL-1542

(19) M. Stern, Thesis, UCRL-1440

(20) W. Powell, UCRL-1191

(21) R. R. Wilson, Phys Rev 53, 408 (1937)

(22) L. R. Henrich, D. C. Sewell, J. Vale, UCRL-353

(23) D. R. Hamilton, H. J. Lipkin, Rev Sci Inst 22, 783 (1951)

(24) B. Rossi and K. Greison Rev Mod Phys 13, 240 (1941)

(25) W. J. Knox, Phys Rev 81, 693 (1951)

(26) D. Bohm and L. Foldy, Phys Rev 72, 649 (1947)

(27) E. Siegbahn and E. Born, Arkiv Mat Astron Fysik 30B, No. 3

(28) R. L. Aamodt, V. Peterson, and R. Phillips, UCRL-1480

(29) E. D. Courant, USAEC NYO-969

(30) See, for example, J. D. Strong, Procedures in Experimental Physics Prentice Hall (1938)

(31) R. Jastrow and I. L. Karp - private communication

(32) W. E. Parkins and E. C. Critenden, Jour App Phys 17, 447 (1946)

(33) N. Bloembergen and P. J. vanHeerden, Phys Rev 83, 561 (1951)

XI. FIGURE CAPTIONS

1. Experimental layout.

2. Available range for observation of recoil deuteron.

3. Energy spectrum of incident protons.

4. Effect of radial oscillation on radius of curvature or energy at which ion strikes target.

5. A comparison of actual range with that computed from geometry. The ordinate is essentially the Y-coordinate on the plate which is 1.41 times the range in copper in millimeters. The abscissa are the channel numbers.

6. Sketch of detector unit.

7. (a) Range spectrum.

   (b) Results of experiment to determine nuclear absorption loss correction.

8. Energy spectra of deuterons from CD_2 and CH_2 targets. Abscissa, deuteron energy. Ordinate, number of tracks.

9. The geometry for computing the acceptance volume element ΔV.

10. The detector system, top cover removed.

11. Alignment template in use.

12. Set of over-exposed nuclear plates illustrating the performance of the detector system.

13. Beam clipper and target support mechanism.

14. Relation of alignment template to orbit geometry.

15. (a) Momentum relations between laboratory and center of mass system.

    (b) Vector diagram of the momenta involved in the pick-up collision leading to the situation shown in (a).

16. Final data, the results of individual runs at the three energies. Abscissa, the center of mass angle θ; ordinate $d\sigma/d\Omega$ center of mass system.

17. Final data as weighted average of individual runs. Abscissa and ordinate same as Fig. 16.

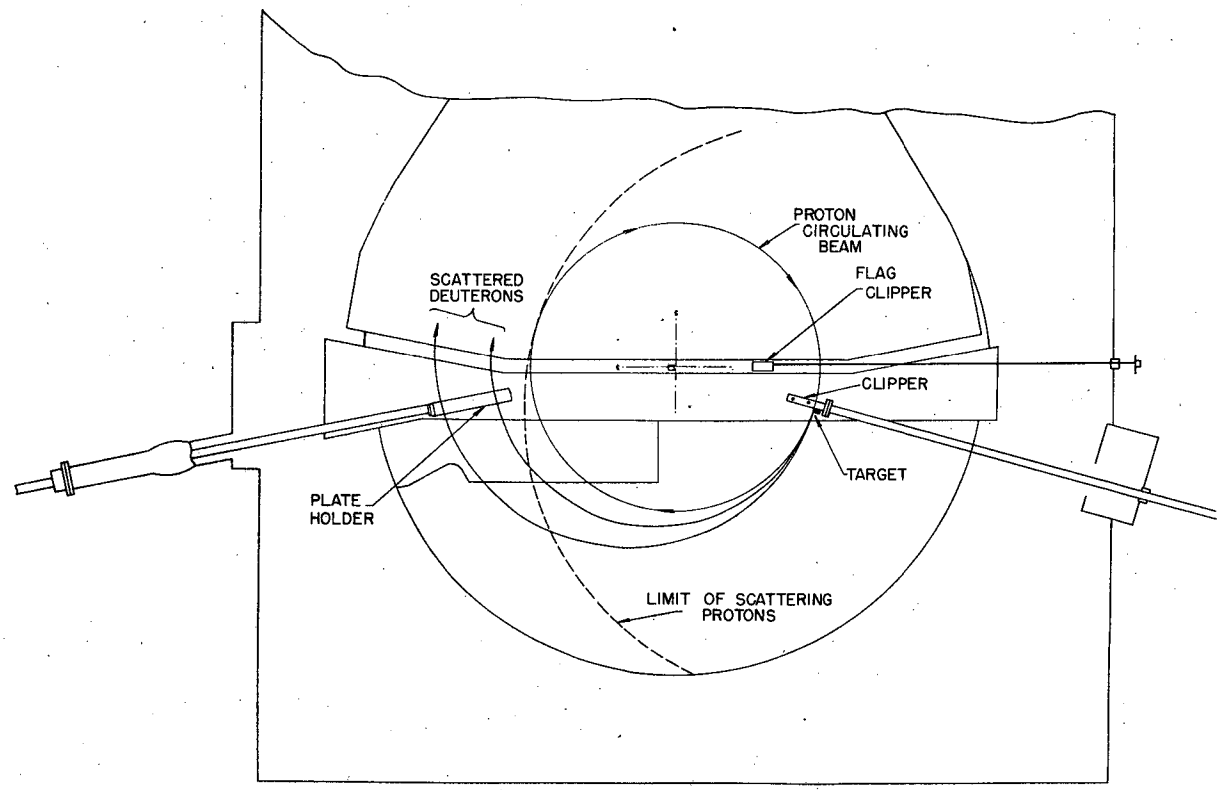
PROTON
CIRCULATING
BEAM
SCATTERED
DEUTERONS
FLAG
CLIPPER
CLIPPER
TARGET
PLATE
HOLDER
LIMIT OF SCATTERING
PROTONS

Fig. 1

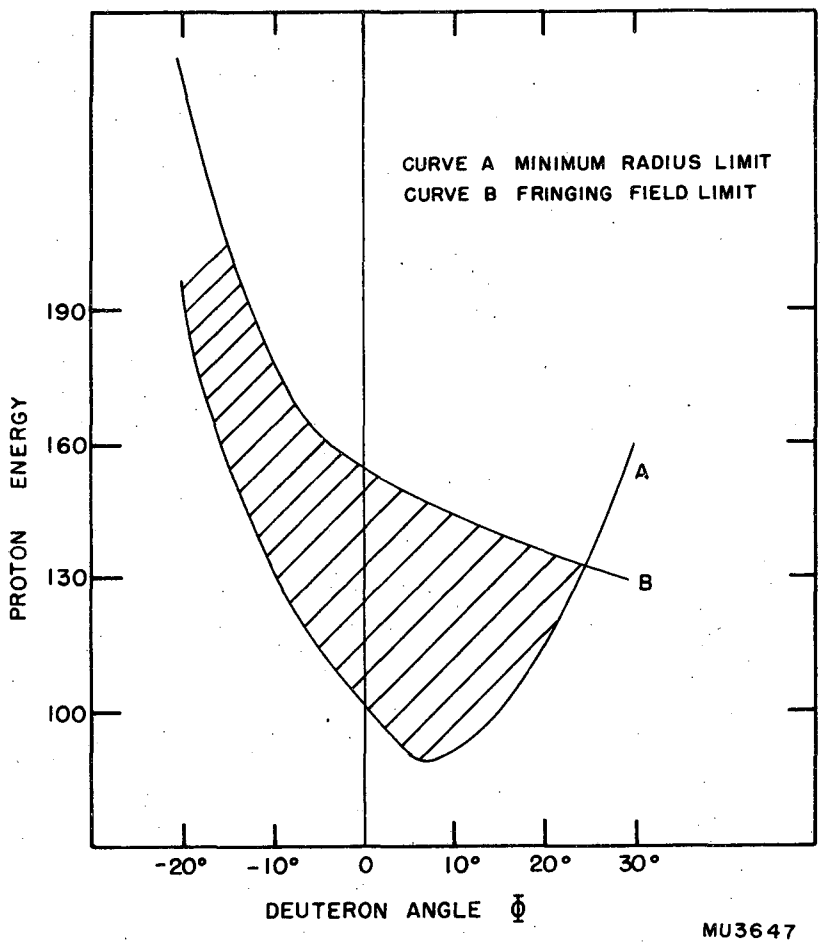
CURVE A MINIMUM RADIUS LIMIT
CURVE B FRINGING FIELD LIMIT
PROTON ENERGY
190
160
130
100
A
B
-20°
-10°
0
10°
20°
30°
DEUTERON ANGLE Φ
MU3647

FIG. 2

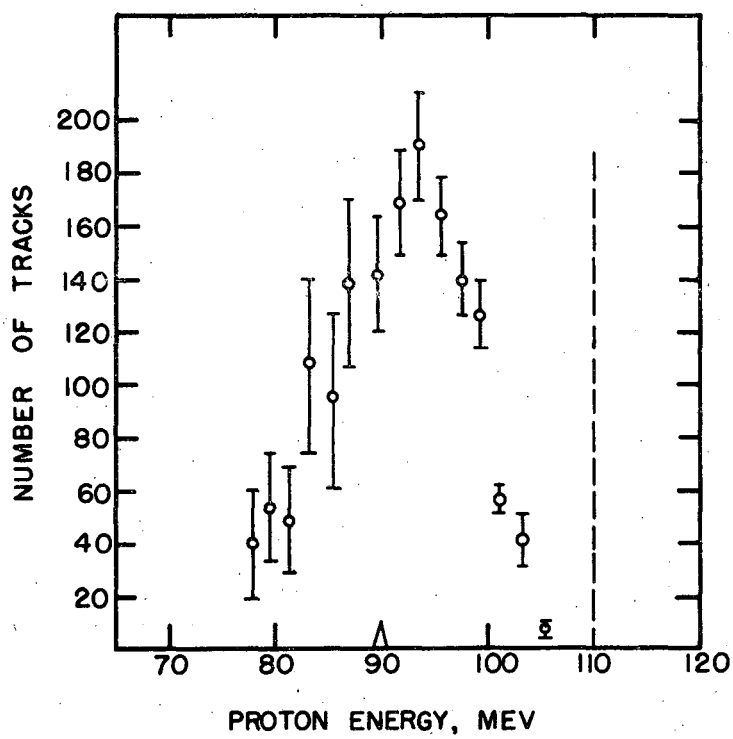
NUMBER OF TRACKS
200
180
160
140
120
100
80
60
40
20
70
80
90
100
110
120
PROTON ENERGY, MEV

FIG. 3

MU3659

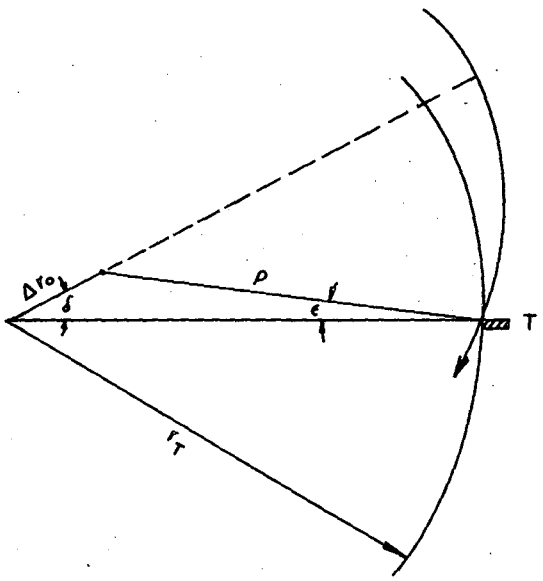

FIG. 4

MU3648

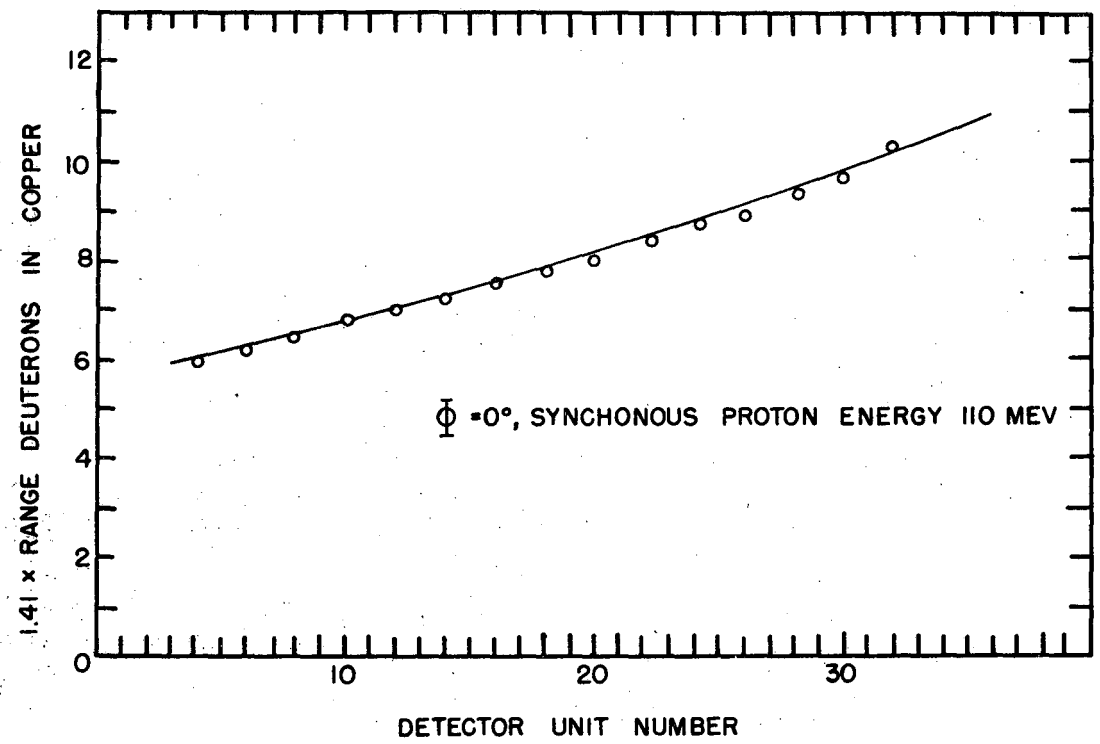
1.41 x RANGE DEUTERONS IN COPPER
0
2
4
6
8
10
12
10
20
30
DETECTOR UNIT NUMBER
Φ =0°, SYNCHONOUS PROTON ENERGY 110 MEV
MU3660

FIG. 5

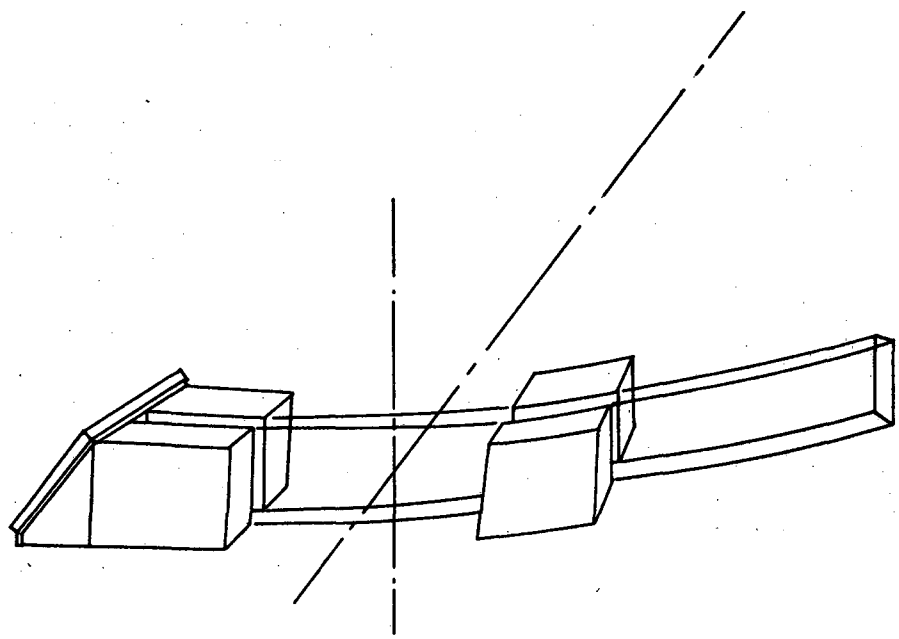

MU3651

FIG. 6

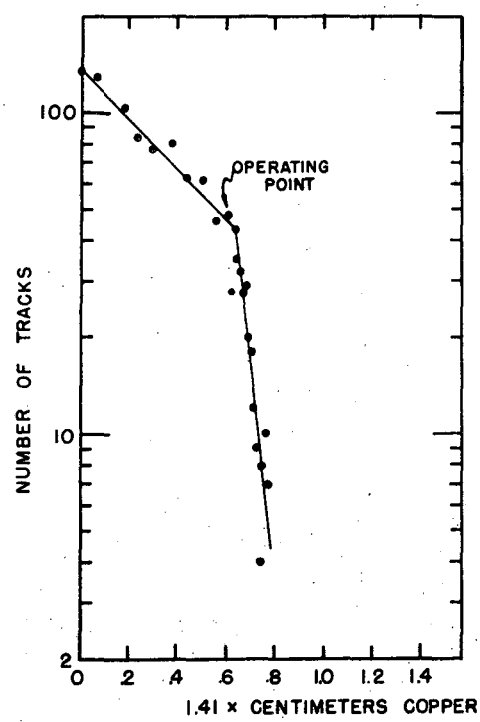

FIG. 7(a)

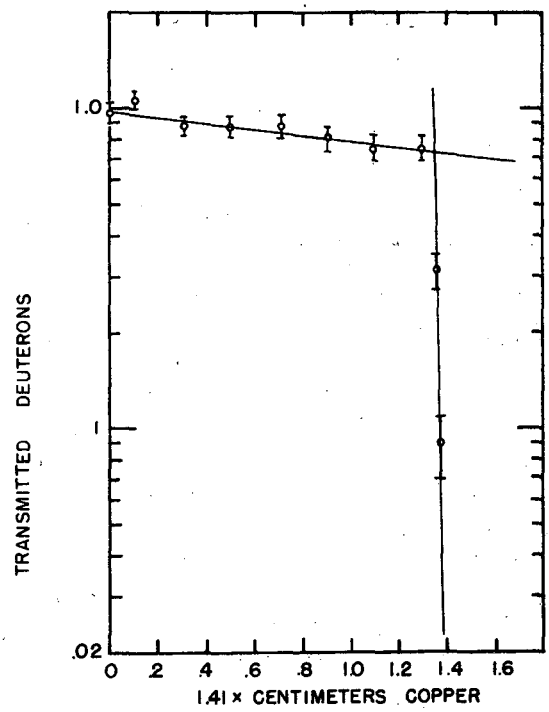

FIG. 7 (b)

MU3661

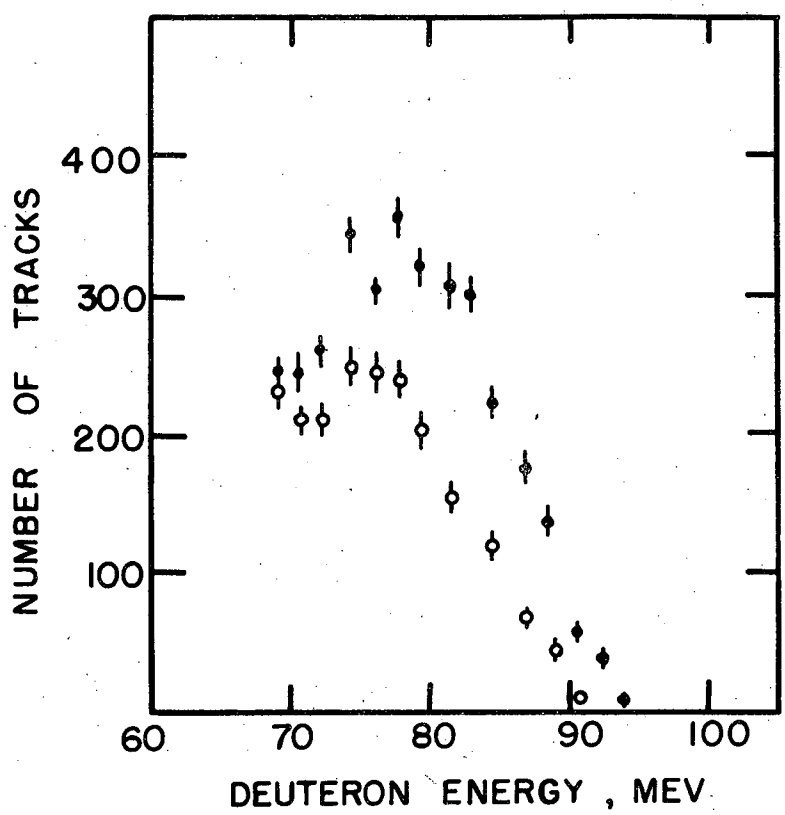
NUMBER OF TRACKS
400
300
200
100
60
70
80
90
100
DEUTERON ENERGY , MEV

FIG. 8

MU3664

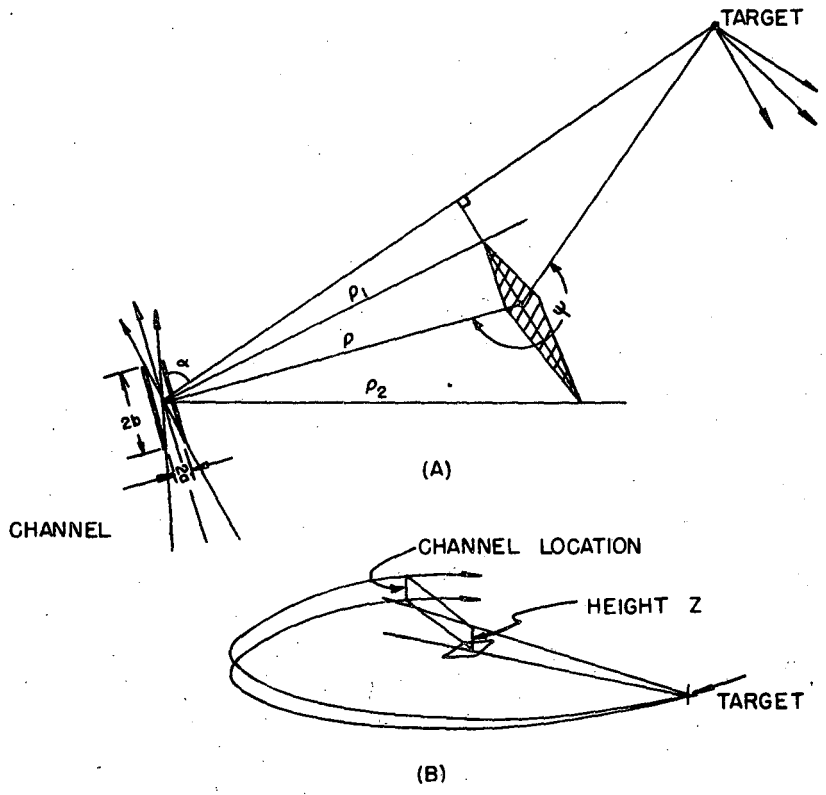
TARGET
ρ_1
ρ
ρ_2
ψ
α
2b
CHANNEL
(A)
CHANNEL LOCATION
HEIGHT Z
TARGET
(B)

FIG. 9

MU3649

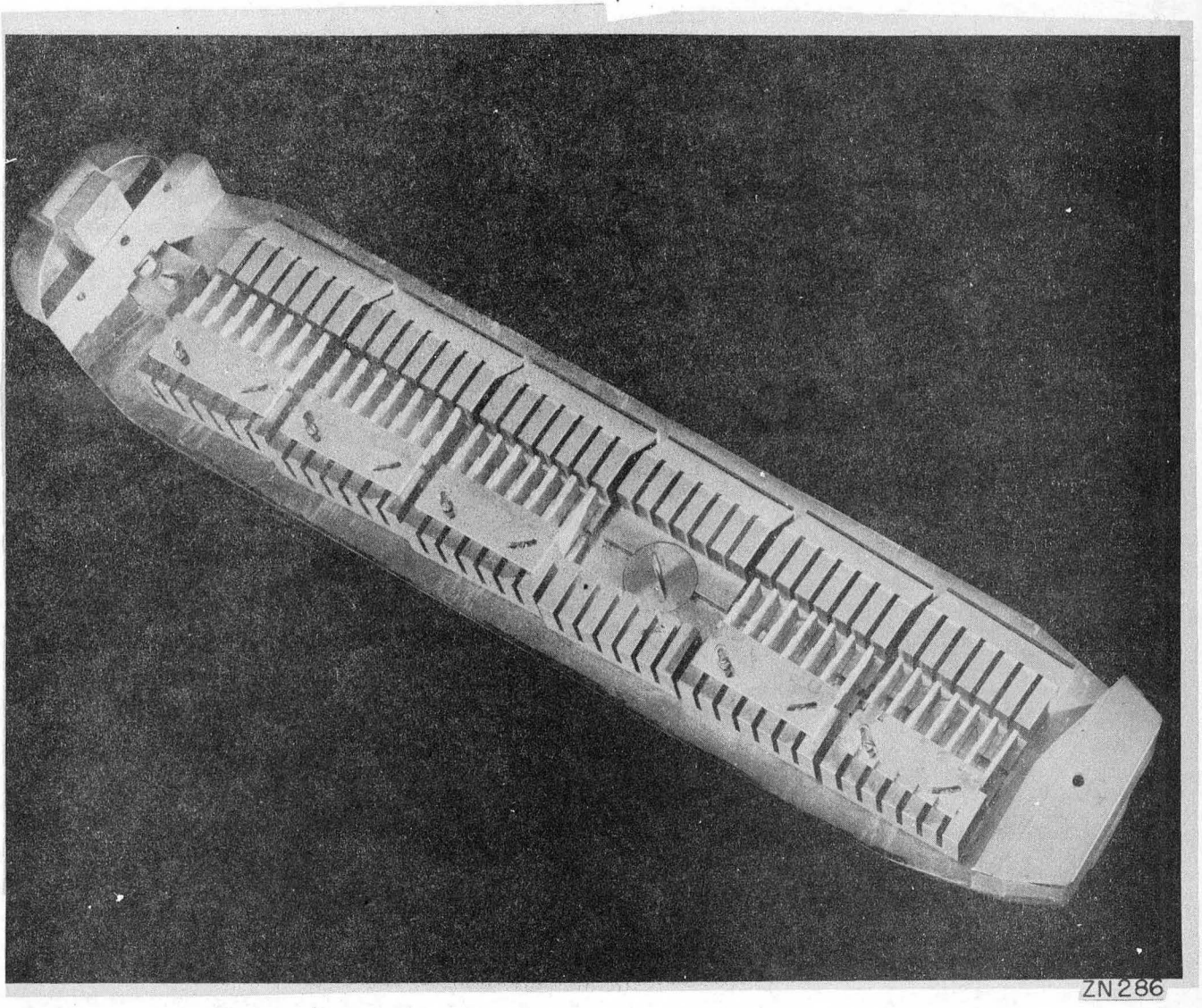

Fig. 10

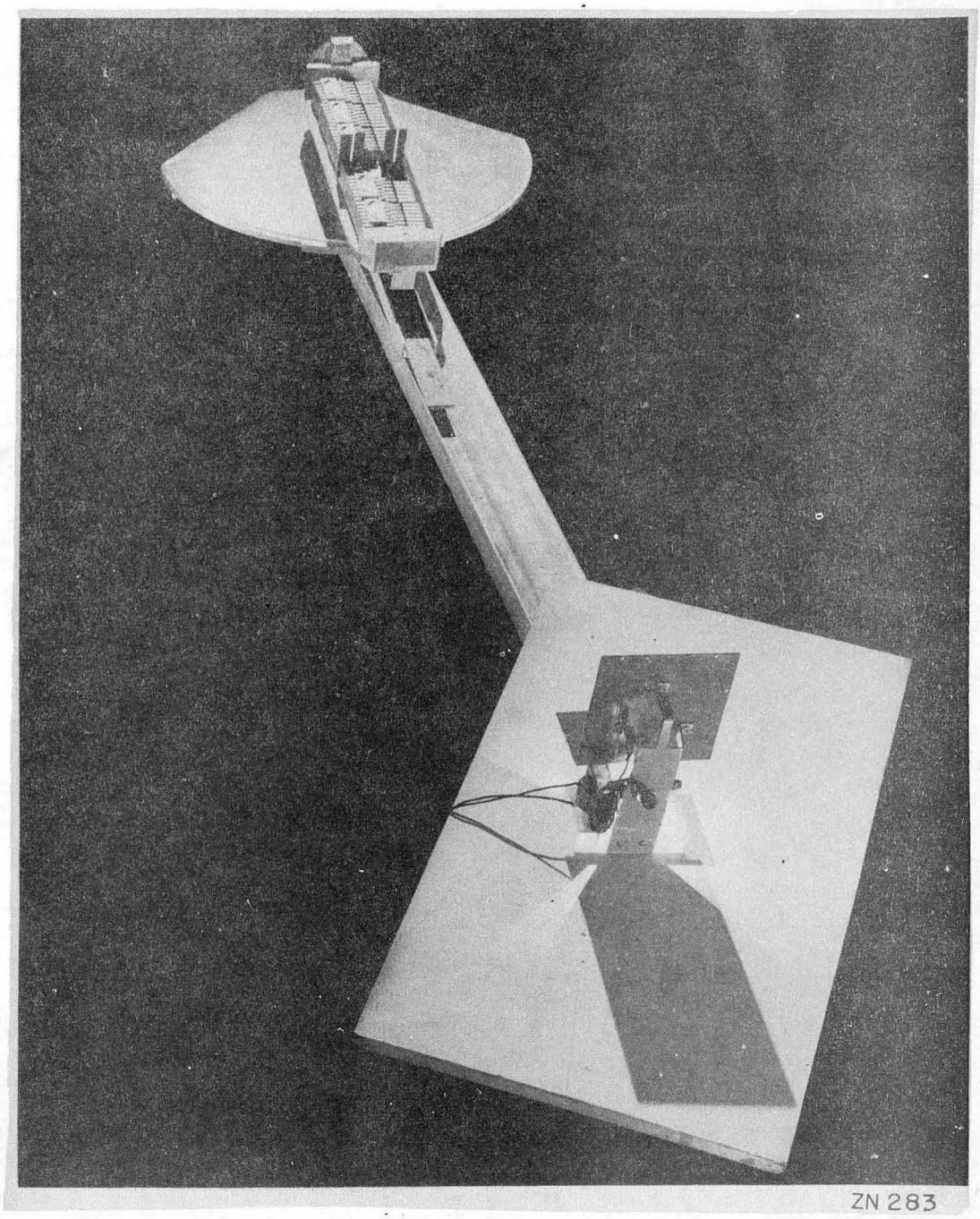

Fig. 11

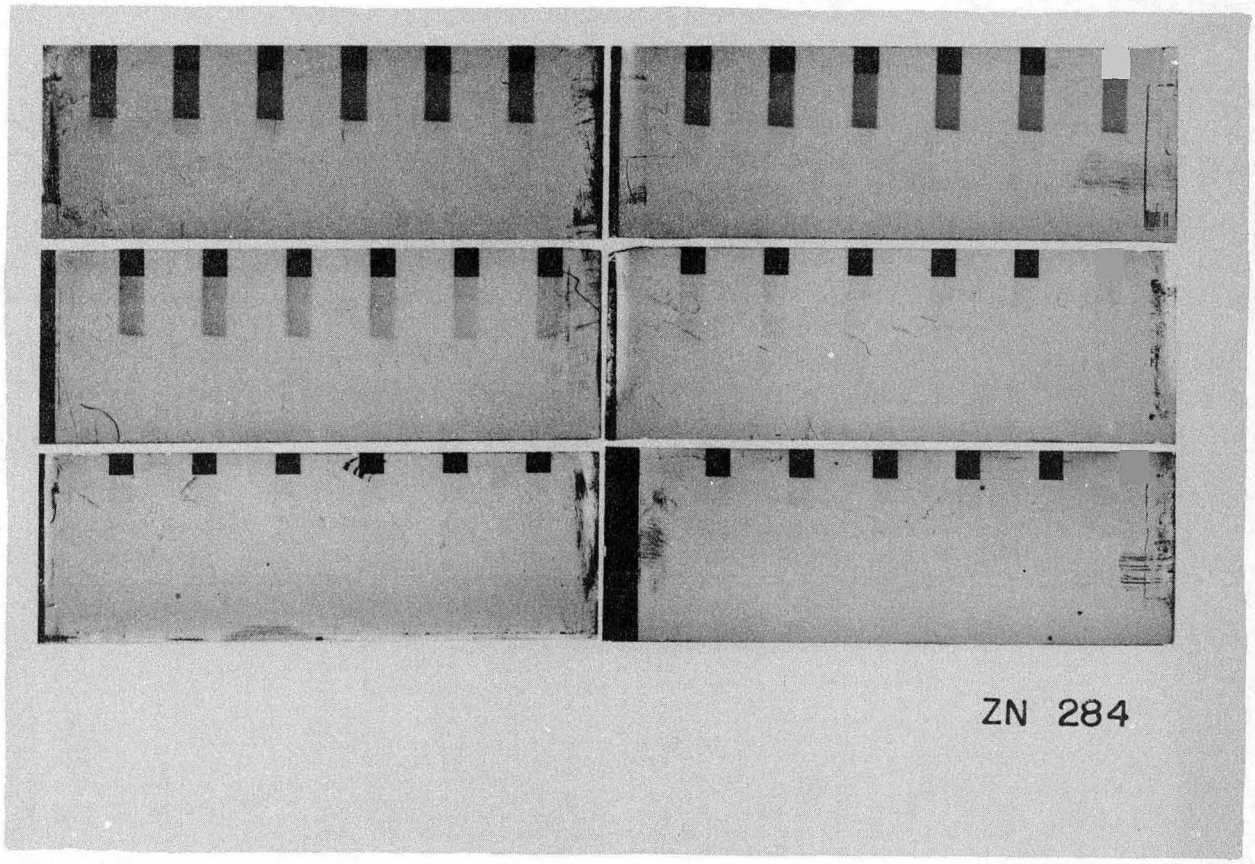

Fig. 12

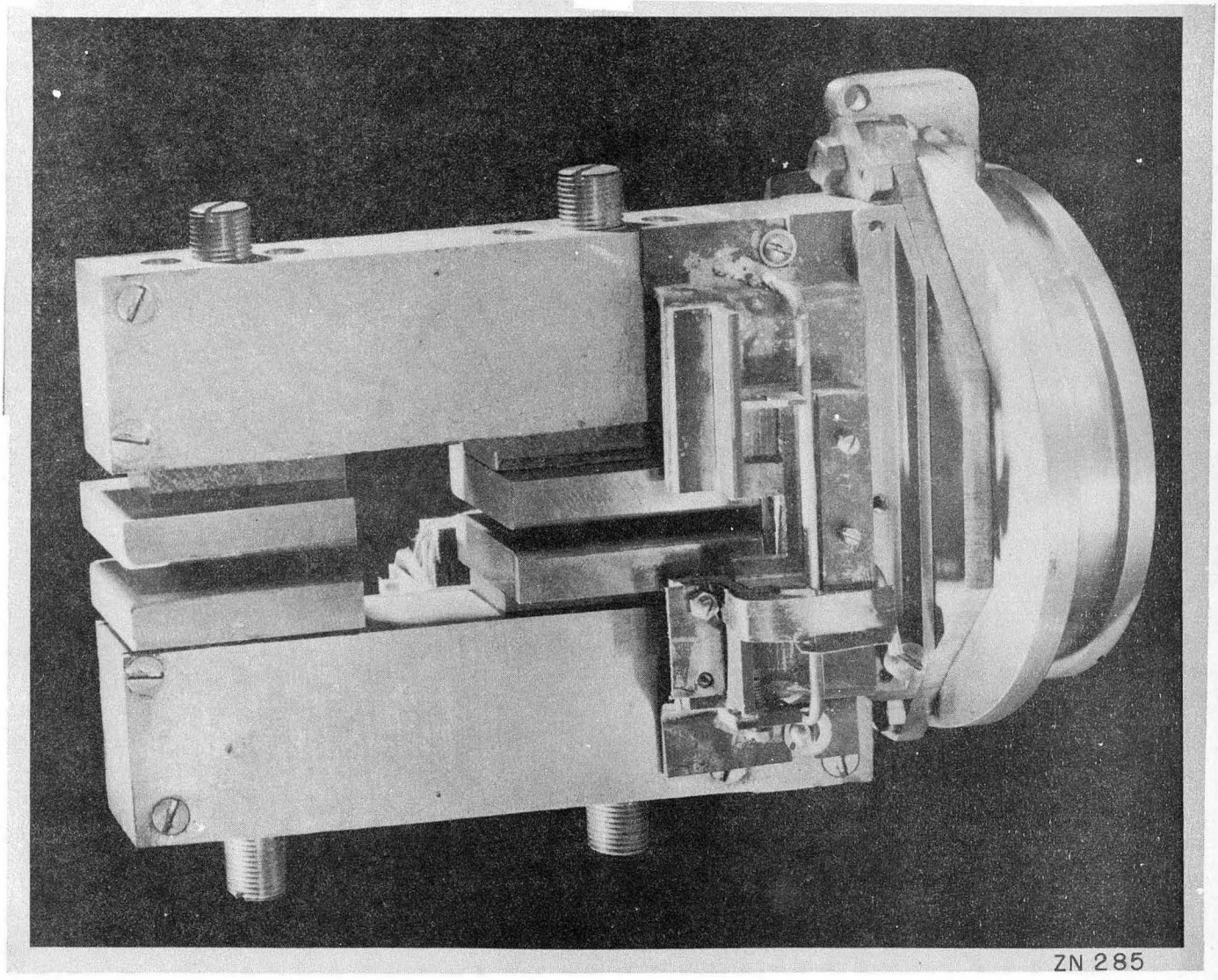

Fig. 13

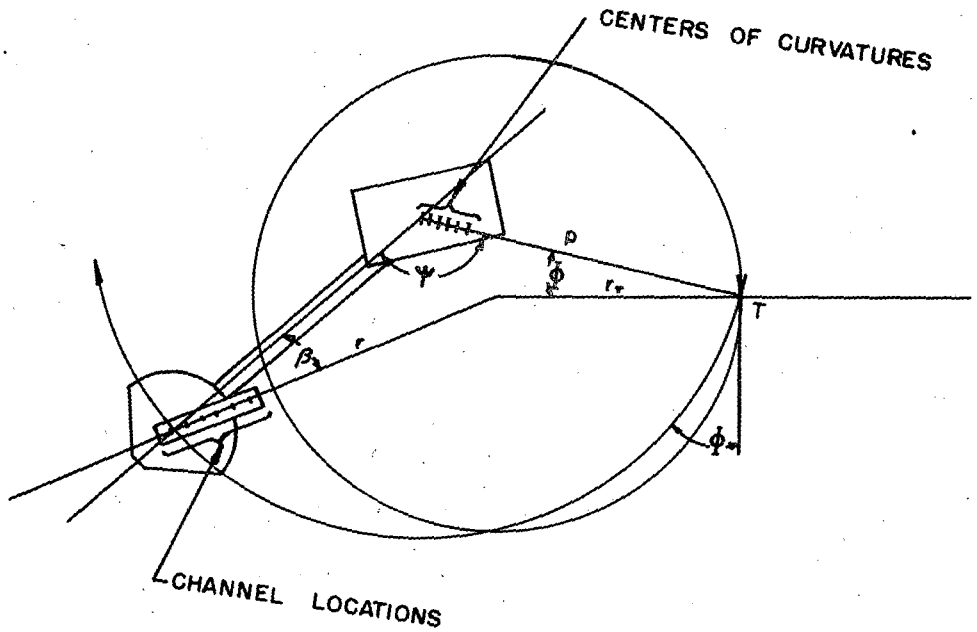

FIG. 14

MU3662

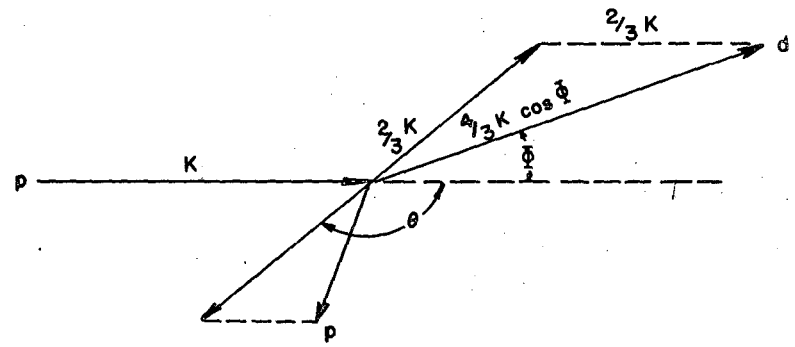

(a)

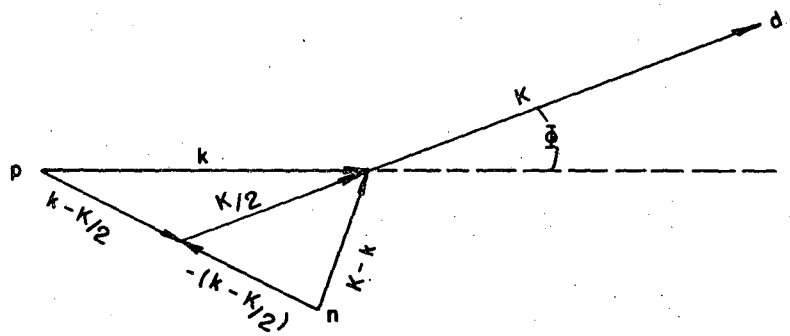

(b)

MU3688

FIG. 15

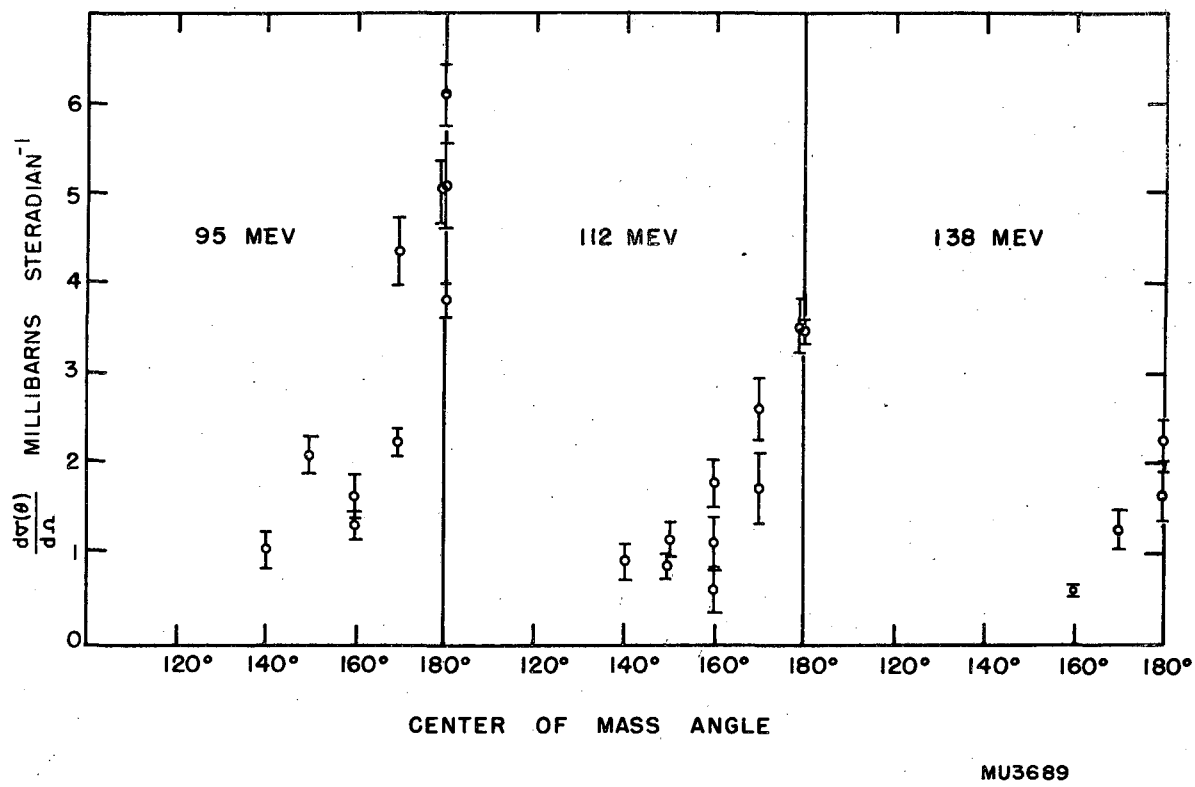
95 MEV
112 MEV
138 MEV
$\frac{d\sigma(\theta)}{d\Omega}$ MILLIBARNS STERADIAN^{-1}
0
1
2
3
4
5
6
120°
140°
160°
180°
CENTER OF MASS ANGLE
MU3689

FIG. 16

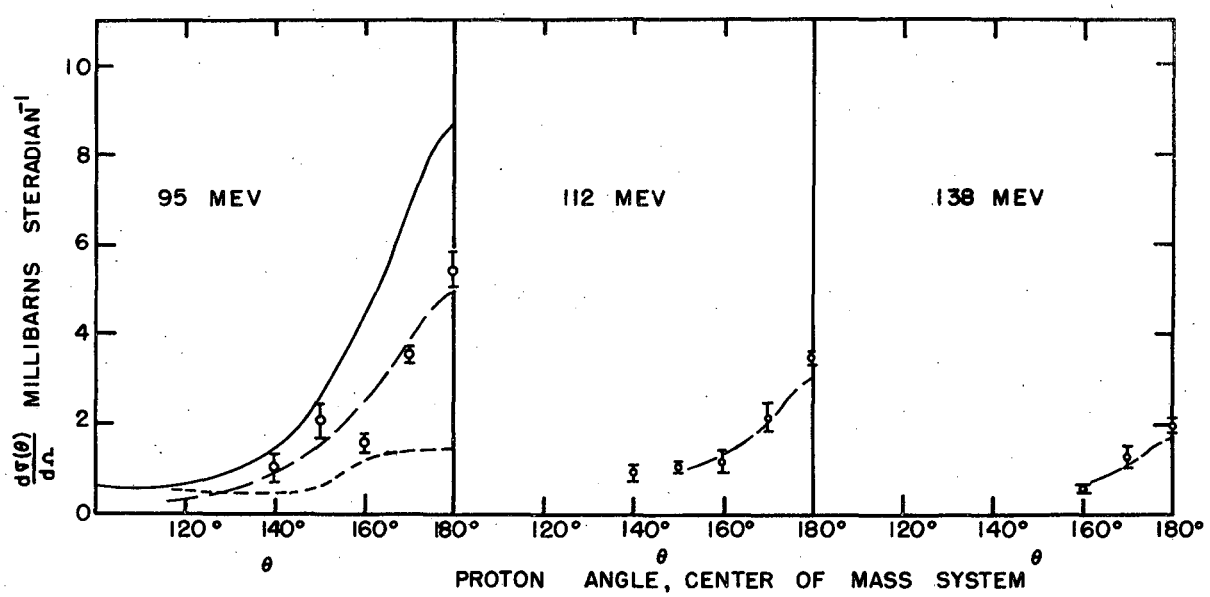

FIG. 17

MU3690